Reaction ^{48}Ca+^{208}Pb: the capture-fission cross-sections and the mass-energy distributions of fragments above and deep below the Coulomb barrier

E. V. Prokhorova, E. A. Cherepanov, M. G. Itkis, N. A. Kondratiev,
E. M. Kozulin, L. Krupa, Yu. Ts. Oganessian and I. V. Pokrovsky
Flerov Laboratory of Nuclear Reactions,
Joint Institute for Nuclear Research,
141980, Dubna, Moscow region, Russia

V. V. Pashkevich
Bogoliubov Laboratory of Theoretical Physics,
Joint Institute for Nuclear Research,
141980, Dubna, Moscow region, Russia

A. Ya. Rusanov
Institute of Nuclear Physics of the National Nuclear Centre of Kazakhstan,
480082 Alma-Ata, Kazakhstan
(Dated: February 8, 2008)

arXiv:nucl-ex/0309021v1 29 Sep 2003

The capture-fission cross-sections in an energy range of $206 - 242$ MeV of ^{48}Ca-projectiles and mass-energy distributions (MED) of reaction products in an energy range of $211-242$ MeV have been measured in the ^{48}Ca+^{208}Pb reaction using the double-arm time-of-flight spectrometer CORSET. The MEDs of fragments for heated fission were shown to consist of two components. One component, which is due to classical fusion-fission, is associated with the symmetric fission of the ^{256}No compound nucleus. The other component, which appears as "shoulders", is associated with the quasi-fission (QF) process and can be named "quasi-fission shoulders". Those quasi-fission shoulders enclose light fragments whose masses are $\approx 60 - 90$ a.m.u. The total kinetic energy (TKE) of the fragments that belong to the shoulders is higher than the value expected for a classical fusion-fission (FF) process. We have come to the conclusion that in quasi-fission, spherical shells with $Z = 28$ and $N = 50$ play a great role. It has also been demonstrated that the properties of the MEDs of fragments formally agree with the standard hypothesis of two independent fission modes; in this case the modes are normal fusion-fission and quasi-fission processes. In this work, a version of the model based on the Dinuclear System (DNS) concept has been developed, which made it possible to describe the experimental energy dependences of the capture-fission cross-sections and the xn-channels of the reaction. The model takes into account shell effects and qualitatively predicts the mass distributions (MDs) for quasi-fission process. A high-energetic Super-Short mode of classical fission has been found at low excitation energies in the mass range of heavy fragments $M = 130 - 135$ and $TKE \approx 233$ MeV; however the yield associated with this mode is small. Its properties can be explained in the framework of the classical modal approach based on the valley structure of the potential energy surface in the deformation space of the fissioning nucleus.

PACS numbers: 21.10.-k, 25.85.-w, 27.90.+b

I. INTRODUCTION

In recent several years, considerable progress has been made in experiments on the synthesis of superheavy elements. New isotopes of the nuclei with $Z = 102 - 116$ were discovered (for example [1-3]). Of particular interest are fusion reactions of ^{48}Ca ions with various heavy targets because of the possibility of producing neutron-rich superheavy nuclei, which, according to theoretical calculations [4], are the most stable nuclei. In three such reactions, namely ^{48}Ca(^{238}U,3n)^{283}112, ^{48}Ca(^{244}Pu,3n)^{289}114, ^{48}Ca(^{244}Pu,4n)^{288}114, and ^{48}Ca(^{248}Cm,4n)^{292}116 long-lived isotopes were produced of element 112 and, for the first time, of elements 114 and 116 [2, 3].

However, as known, the excited superheavy systems produced in reactions with massive heavy ions undergo fission or competitive quasi-fission, which are their dominant decay channels and whose characteristics carry information on collision dynamics, the life and decay of the composite nucleus. The relation between the contributions of fission and quasi-fission to the total ion-target interaction cross-section depends quite strongly on the charges Z_i, Z_t and masses A_i, A_t of the ion and target involved. For example, for the reaction ^{48}Ca+^{208}Pb, the fission of the compound nucleus of ^{256}No [5] is the main decay process, whereas in the reaction ^{48}Ca+^{238}U, quasi-fission, a process in which no classical compound nucleus is formed, dominates [6-8].

We studied both of those reactions for the energies of bombarding ^{48}Ca-ions near and below the Coulomb barrier of interacting partners. In this work, we report on the experimental results obtained for the reaction ^{48}Ca+^{208}Pb: on

the capture-fission cross-sections and structural peculiarities of the mass-energy distributions (MEDs) of the fission fragments of the excited compound nucleus ^{256}No. We also proposed a version of the model based on the Dinuclear System concept, which describes competition between fusion-fission and quasi-fission processes.

Recently, that reaction has already been studied in a few works: in [5, 9, 10], the capture-fission cross-sections were measured, and, in [5, 11], the MEDs of fragments. Our interest in it is connected with the fact that the possibility has emerged of investigating the characteristics of that reaction deep below the Coulomb barrier, where a compound system of quite low excitation energy (cold fusion reactions [12]) can be produced, which is unattainable in other ion-target combinations. Such experiments were made possible by modernisation of the FLNR U-400 accelerator ion source, which enabled the production of ^{48}Ca-ion beams of high quality and required energy [13], and by development of the double-arm time-of-flight wide-aperture spectrometer CORSET [14], with whose help the velocities and coordinates of nuclear reaction products produced with record low cross-sections can be measured with a sufficiently high resolution [15]. Some preliminary results of those experiments were presented in brief reports [16, 17].

II. MEASURING TECHNIQUE AND DATA PROCESSING

The experiment was carried out on the extracted beam of the U-400 accelerator at the Flerov Laboratory of Nuclear Reactions, Dubna. The capture-fission cross-sections were measured in the range of the energies of bombarding ^{48}Ca ions from 206 to 242 MeV; the MEDs of reaction products were measured in the range $211 - 242$ MeV. The target was a 220 μg/cm^2 ^{208}Pb layer deposited on a 50 μg/cm^2 carbon backing foil.

To register reaction products, the well known kinematic coincidence method [5-8, 10,18] was applied with the use of the double-arm time-of-flight spectrometer CORSET [14]. Each arm of the CORSET spectrometer consisted of a start detector composed of microchannel plates with an electrostatic mirror and two stop position-sensitive (x, y-sensitivity) detectors also composed of microchannel plates, 6×4 cm in size. The start detectors were positioned at a distance of 3.5 cm from the target. The minimum start-stop flight distance was 11.5 cm. Thus, the spectrometer consisted of two start detectors and 4 stop detectors and covered a solid angle of 360 msr. The position resolution of the stop detectors was 0.7 mm. The mass resolution of the spectrometer was checked against the MEDs of fragments for the spontaneous fission of ^{252}Cf; our estimate of it is $3 - 5$ u. [19]. Each arm of the spectrometer could be independently moved along the radius of the reaction chamber without vacuum failure, so that the arms could be installed at selected correlation angles. The technique used to measure the capture-fission cross-sections for different correlation angles was the same as described in work [10]. To absolutely normalise cross-sections and to monitor the ion beam, two semiconductor monitors capable of registering elastically scattered ions of ^{48}Ca were installed at angles of $\pm 11^\circ$.

To measure MEDs of reaction products, the spectrometer arms were positioned at correlation angles of 57° and 78° correspondingly. The registering angles in the laboratory system were $\theta_{\rm lab1} = 39^\circ - 75^\circ$ and $\theta_{\rm lab2} = 61^\circ - 95^\circ$, which corresponds in center-of-mass system for registerated products to $\theta_{\rm CM1} = 47 - 113^\circ$, $\theta_{\rm CM2} = 73^\circ - 140^\circ$. In this case, the spectrometer was capable of registering all reaction products with the mass of from a bombarding ion to target nuclei. The experiment geometry is schematically depicted in Fig. 1. Since the spectrometer acceptance did not allow the whole range of energy-mass ratios to be registered with the same probability, corrections for its geometrical efficiency were introduced. As an example, a two-dimensional map (in percent) of that efficiency in mass-energy coordinates is presented in Fig. 2 for the bombarding energy $E_{\rm lab} = 242$ MeV. That map was calculated by the Monte-Carlo method proceeding from the two-body nature of the reaction exit channel.

The data were processed by the standard technique; for details, see works [7, 8, 18]. Energy losses of reaction products in the target layer, backing foil and in electron emitters of the start detectors were taken into account. The spectrometer was calibrated in two stages. At the preliminary stage, the spectrometer arms were positioned opposite each other and ^{252}Cf fission fragments were used to calibrate the spectrometer. At the final stage, the arms were in the operating position and the calibration was carried out of the energy of registered elastically scattered ions of ^{48}Ca and ^{208}Pb. Particular attention was given to the angular folding correlation of products both in and out of the reaction plane. Only those events which correspond to the two-body process of complete momentum transfer were selected and then analysed. Let us give a typical example of such selection.

Figure 3 shows the two-dimensional matrix $(M - TKE)$ (mass of reaction products and their total kinetic energy) for all the registered events, that is, summed over all the measured angles, for the energy of ^{48}Ca bombarding ions $E_{\rm lab} = 242$ MeV on the assumption that all the events are two-body events. Fig. 4 presents the two-dimensional matrices for those events as a function of the sum of the angles in the center-of-mass system in the reaction plane $\Theta_{\rm CM}$ and out-of-plane $\Psi_{\rm CM}$; Fig. 4(a) presents the matrices for all the events; Fig. 4(b) only for the fission fragments extracted from the matrix $(M - TKE)$ as shown in Fig. 3. It is clearly visible that for fragments (Fig. 4(b)), matrix $(\Theta_{\rm CM} - \Psi_{\rm CM})$ is quite symmetric around 180° in both planes, only few events are located to the right from it, which points to fission occurring after incomplete momentum transfer. We only took account of the events lying within the contours indicated in Figs. 4(a) and 4(b). In Fig. 4(a), there is a different situation for all the registered events. It

is clearly visible that the distribution is extended toward the large angles in the reaction plane, which is evidence of a quite major contribution due to a non-two-body process that does not result to the capture and fission in the peripheral interaction of colliding partners. In Figs. 4(c), (d), (e) and (f), the same data are represented in a more illustrative way and in the $(\Theta_{\rm CM} - TKE)$ coordinates; Fig. 4(c) presents all the registered event; Fig. 4(d) only shows the fragments. In Figs. 4(e) and 4(f), the selected events from within the contours in Figs. 4(a),(b) are shown in the same coordinates. Later on, the events confined in the contours in Figs. 4(a),(b) were only analysed. The same procedure was applied for the other energies of ^{48}Ca-projectiles.

Thus we managed to separate quite reliably the two-body process of system decay from the background of all other reaction channels and then we could extract physical information only from the events, corresponding to the above mentioned criteria.

III. RESULTS

Table I gives the parameters of the studied reactions and some measured integral characteristics of fragments.

At the top of Fig. 5, the capture-fission cross-section is shown as a function of the excitation energy of the compound nucleus E^*. Our results are in good agreement with the data from works [5,10], which are also shown in Fig. 5. At the bottom of that figure, the data are presented on the cross-sections of the xn-channels of the reaction under study from work [20]. With solid curves, the description is shown of those data on the basis of the Dinuclear System Model, which is to be discussed in detail later on. The dotted curve represents the cross-section for the complete fusion of ^{48}Ca and ^{208}Pb ions also calculated on the basis of that model.

Figures 6, 7 and 8 demonstrate the MEDs of reaction products for all the studied energies of ^{48}Ca ions. Shown from top to down in those figures are: the two-dimensional matrices $(M - TKE)$, mass distributions and next, only for fragments, the TKE and its variance $\sigma^2_{\rm TKE}$ as functions of fragment mass.

Figure 6 gives the measured results for the MEDs of fragments for the four largest values of the energy of ^{48}Ca-ions. The reaction products near the masses of bombarding ion and target ($\cong M_{i,t} \pm 20$) are easy to identify as elastic, quasi-elastic and deep inelastic events. At the same time, it is clearly visible that the fragment mass distributions for symmetric masses with $A/2 \pm 30$ are of a shape close to a gaussoid and that the dependences of $\langle TKE\rangle(M)$ and $\sigma^2_{\rm TKE}(M)$ are of parabolic shapes. It is this behaviour of the indicated characteristics of fragments that is typical of the fission of heated nuclei, as predicted by the liquid-drop model (LDM) [21] or the diffusion model [22], since the shell properties of a fissioning nucleus become not essential, that is, their distinctive features are inherent in standard classical fission. At the same time, for light fragments with masses $65 \leq M \leq 100$ and the masses complementary to those values, the mass distributions show "shoulders"; those "shoulders" are due to fact that the yield of reaction products increases in comparison with that predicted for classical fission. Each of those events can hardly be thought to be a deep inelastic process as well because they belong in the matrix of fragments, that is, they are fragment-like, although to the right and the left of that region, smooth transition is seen to events of deep inelastic transfer and to standard fission, and, on the whole, it is impossible to conclusively indicate the boundary of "shoulders". It should be noted that in Fig. 6, the "shoulders" are sufficiently easy to separate from the main symmetric peak of fragments for the ion energy $E_{\rm lab} \leq 232$ MeV but no longer easy to separate for the energy $E_{\rm lab} = 242$ MeV and one can judge about their presence from the sharp widening of the MD bottom. In Fig. 6, in the region of fragment masses in which the "shoulders" dominate an increased TKE is seen for all the four ion energies as compared with "normal" fission. However, the data presented in Fig. 6 are not statistically accurate enough to state that the fragment characteristics for the masses in the region of "shoulders" are different from classical fission. To clarify this issue, which, in our opinion, is a principal one, we once again measured the MEDs of fragments for the energy of ^{48}Ca ions $E_{\rm lab} = 230$ MeV with statistics of events of about one order higher than those on the average in Fig. 6. The results of that experiment are shown in Fig. 7. It is clearly visible that, indeed, for light fragments of the masses $M_L \leq 95$ and the heavy masses complementary to them, the TKE obviously deviates upwards from the parabolic curve by which the dependence $\langle TKE\rangle(M)$ is well described in the region of symmetric masses. It is also seen that a small wide maximum, invisible in the same distributions in Fig. 6, becomes faintly visible in the $\sigma^2_{\rm TKE}(M)$ dependence in the range of symmetric mass $M = 115 - 140$. This means that though it is close to liquid-drop fission in properties, the fission of ^{256}No at $E_{\rm lab} = 230$ MeV ($E^* = 33$ MeV) has insignificant structural peculiarities characteristic of enough low-energy fission that do not manifest themselves directly in the mass yields and the TKE of symmetric fission fragments.

Recall that no "shoulders" are observed in the MEDs of the compound nucleus of ^{255}No produced in the reaction ^{16}O+^{239}Pu, which is also true for the fissioning nuclei that are produced in reactions with "light" heavy nuclei, and which are close to that nucleus. In addition, the dependences $\langle TKE\rangle(M)$ and $\sigma^2_{\rm TKE}(M)$ show no peculiarities [23]. Then we will use the term "quasi-fission shoulders", without going into detail yet, in reference to the light fragments with $M \leq 95$ and the heavy masses complementary to them.

Figure 8 gives the MEDs of fragments for the two lowest energies of ^{48}Ca ions $E_{\rm lab} = 217$ and 211 MeV, which cor-

responds to the initial excitation energy of the compound nucleus of ^{256}No $E^* = 22,5$ and $17,6$ MeV correspondingly. At those E^*, according to systematics [24], practically no pre-fission neutrons are emitted (see Table I) and, therefore, the actual temperature E^* with which the nucleus breaks up is not different from the initial temperature. Those are rather low excitation energies, and in Fig. 8, it is clearly visible that the shape of the MD is far from a gaussoid: there are structured flat tops in the region of the heavy masses $M_H \cong 128-135$, and at the lowest energy ($E_{\rm lab} = 211$ MeV) there is, in addition, a clearly defined increased yield of fragments for $M_H = 145-155$. For the fragment masses near $A/2$ at $E_{\rm lab} = 217$ MeV, in contrast to higher energies, the distribution $\langle TKE\rangle(M)$ is obviously extended toward the larger TKE. That makes the impression that the wide parabolic dependence $\langle TKE\rangle(M)$, characteristic of the fission of more heated nuclei (Fig. 6 and 7), has a narrow more high-energetic component. For the energy $E_{\rm lab} = 211$ MeV, only this narrow component basically remains, and here the dependence $\sigma^2_{\rm TKE}(M)$ shows a statistically significant spike in the variance. That the MEDs of fragments presented in Fig. 8 behave in such a manner points to the fact that shell effects manifest themselves in the quite low-energy fission of the compound nucleus of ^{256}No.

IV. MODEL

A. Fundamentals of the Dinuclear System Concept

The motivation for the DNS Concept (DNSC) and a comparison of the DNS Concept with existing models for the fusion of massive nuclei have been already given in works [25-28]. Therefore here we will only discuss its main features applied to analysis of the fusion reactions used in the production of transfermium elements. According to the DNS concept, complete fusion occurs as follows. At the capture stage, after the kinetic energy is completely transferred into the inner degrees of freedom, a dinuclear system is formed with the capture cross-section σ_c. The capture cross-section σ_c is part of the total inelastic cross-section σ_R:

$$\frac{\sigma_c}{\sigma_R} = \left[\sum_{l=0}^{l_{cr}} (2l+1)T(l,E_{CM})\right] / \left[\sum_{l=0}^{\infty} (2l+1)T(l,E_{CM})\right], \tag{1}$$

where l_{cr} is the critical angular momentum at which the heavy ion is captured and the excited dinuclear system is formed. The value for l_{cr} was taken from empirical systematics for the σ_c/σ_R ratio [29]. The capture cross-section is described by the formula:

$$\sigma_c(E^*) = \pi\lambda_0^2 \sum_{l=0}^{l_{cr}} (2l+1)T(l,E_{CM}), \tag{2}$$

where the penetration of the potential barrier is calculated on the basis of the standard inverted parabola method and written as

$$T(l,E_{CM}) = \left\{1+\exp\left[(2\pi/\hbar w)(B-E)\right]\right\}^{-1}, \text{ where } \hbar w = \hbar/\sqrt{\mu}\left[d^2V(R,l)/dr^2\right]^{1/2}, \tag{3}$$

Here E_{CM} is the center-of-mass energy of the bombarding ion; R – the distance between the centres of the nuclei; μ – the reduced mass of the system; B – the Coulomb barrier. In calculating the capture cross-section, the Woods-Saxon potential was used as the interaction potential:

$$V_N(R) = \frac{V_0}{1+\exp\left\{\left[R - r_0\left(A_i^{1/3}+A_t^{1/3}\right)\right]/d\right\}}, \tag{4}$$

whose parameters: d – the diffuseness of the potential, V_0 – the depth of the potential, and r_0 – the radius parameter, were taken from work [29], in which empirical systematics for the parameters of the potential had been found on the basis of a large body of experimental data on the capture cross-section.

In our approach, complete fusion is the final stage of the evolution of a DNS, at which all the nucleons of one nucleus will have gradually been transferred to the other nucleus. In the best known models for nuclear fusion, the production cross-section for compound nuclei, $\sigma_{\rm CN}$, is not different from the capture cross-section, σ_c; in other words, after the capture stage, the compound nucleus is formed with 100% probability. In our approach, the complete fusion

cross-section, $\sigma_{\rm CN}$, is part of the capture cross-section, σ_c. The fusion process will compete with the quasi-fusion process, and therefore the complete fusion cross-section can be written as

$$\sigma_{\rm CN}(E^*) = \sigma_c \cdot P_{\rm CN} \approx \pi\lambda_0^2 \sum_{l=0}^{l_{cr}} (2l+1) T(l, E_{CM}) \cdot P_{\rm CN}, \tag{5}$$

where $P_{\rm CN}$ is the probability that complete fusion will occur.

In the evolution of the DNS, each nucleus of the DNS retains its individuality; this is a consequence of the influence of the shell structure of the partner nuclei since the kinetic energy of the bombarding ion, and, thus, the resultant excitation energy, as a rule, is low in those reactions. The Macroscopic Dynamic Model (MDM) [30] description of the coalescence of two nuclear drops does not take account of the shell structure of the nuclei, and complete fusion does not compete with quasi-fission. Those two processes are considered to be distinctly separated in energy space.

An essential characteristic of a DNS, determining its evolution, is the system's potential energy $U(Z, J)$: $U(Z, J) = B_1 + B_2 + V(R^*, J) - [B_{CN} + V_{\rm rot}(J)]$,

where Z – charge of one of the DNS partners, J – spin of the system, which practically coincides with the angular moment of collision L (further we shall use everywhere L); B_1, B_2 and B_{CN} – binding energies of DNS nucleus and a compound nucleus. $V(R^*, L)$ – the nucleus-nucleus potential taken at point R^* corresponding position of a minimum in potential energy, which includes Coulomb, nuclear and centrifugal potentials:

$$V(R, L) = V_C(R) + V_N(R) + V_{\rm rot}(R, L). \tag{6}$$

We took PROXIMITY (for details, see [31]) as the nuclear potential $V_N(R)$.

$$V_N(R) = 4\pi\gamma \cdot \overline{R} \cdot b \cdot \Phi(\xi) \tag{7}$$

$$\text{where } \gamma = 0.9517 \cdot \left[1 - 1.7826 \left(\frac{N-Z}{A}\right)^2\right] \cdot MeV \cdot fm^2, \quad \overline{R} = \frac{C_P \cdot C_T}{C_P + C_T},$$

$$\text{and } C_i = R_i(1 - b^2/R_i^2 + ...), \quad \xi = s/b, \quad s = r - (C_P + C_T),$$

$$R_i = 1.28A_i^{1/3} - 0.76 + 0.8A_i^{-1/3}, \quad b = 1.0, \quad i = P \text{ or } T$$

$$\Phi(\xi) = \begin{cases} -1.7817 + 0.9270 \cdot \xi + 0.14300 \cdot \xi^2 - 0.09000 \cdot \xi^3, & \xi < 0 \\ -1.7817 + 0.9270 \cdot \xi + 0.01696 \cdot \xi^2 - 0.05148 \cdot \xi,^3 & 0 < \xi < 1.9475 \\ -4.41 \cdot \exp\left(-\frac{\xi}{0.7176}\right), & \xi > 1.9475 \end{cases}$$

The Coulomb energy was calculated from the following formula:

$$V_C = Z_P Z_T e^2 \cdot \begin{cases} 1/r, & r \geq R_C \\ \frac{1}{2R_C}(3 - r^2/R_C^2), & r < R_C \end{cases},$$

where $R_C = r_C(A_P^{1/3} + A_T^{1/3})$

The rotation energy $V_{\rm rot}(R, L)$ was calculated with the solid moment of inertia. Our estimates show that the rotation component has a small effect on the calculation results of competition between fusion and quasi-fission processes for the ion energy close to the Coulomb barrier.

Shown in Fig. 9 is a qualitative picture that presents three-dimensional PROXIMITY potential as a function of the distance between the centres of the nuclei and the charge number of one of the DNS fragments. On capturing a heavy ion by a target nucleus, the formed DNS will fall into a potential pocket. Then the double system will be moving along the valley of the potential pocket both in the direction to symmetry and in the direction to decreasing the charge number of one of the fragments — in the direction to fusion. On the way, the DNS might undergo a break-up into two fragments — QF, i.e. fission without a compound nucleus being produced. In the figure, the corresponding processes are indicated by arrows. In Fig. 10, shown are two profiles of the potential energy: the profiles along the minimum and the maximum of the potential surface calculated for the reaction ^{48}Ca+^{208}Pb. The curve $U(Z, L = 0)$ (for the magnitude of R corresponding to the pocket) has a few local minima, which reflect the shell structure in interacting nuclei. Heavy and superheavy elements (SHE) are typically produced at the ion energies that result in the minimally possible excitation energy of the compound nucleus. This ensures higher survival probability for the compound nucleus while de-excited. In Fig. 10, the DNS energy that corresponds to the minimally possible excitation energy of the compound nucleus is shown by cross-hatching. As follows from Fig. 10, the system will undergo most

heating while descending from the Businaro-Gallone point (B.G.) to the point of compound nucleus formation. Only at this stage of DNS evolution will most of the potential energy of the dinuclear system be transformed into the heat excitation of the compound nucleus. This peculiarity of DNS evolution, characteristic of SHE fusion reactions, required the use of experimental masses to calculate the potential energy $U(Z, L)$. In addition, on the way to the compound nucleus, the DNS should overcome the inner potential barrier $B^*_{\rm fus}$, which is the difference between the magnitudes of the potential energy $U(Z, L)$ at the B.G. and at the reaction entrance point. The inner potential barrier $B^*_{\rm fus}$ results from nucleon transfer in a massive DNS being of an endothermic nature, which makes the system move in the direction to the compound nucleus. The movement of the DNS in the reverse direction, to more symmetry, might result in its leaving the potential pocket (with a break-up into two fragments — the movement in the direction to increasing R) after overcoming the QF barrier, which we took to be the difference between the magnitudes of driving potential for the entrance combination and the point of scission into two fragments. The required energy for overcoming these barriers is taken from the excitation energy E^* of the dinuclear system, which an essential feature of our approach. A compound nucleus is unlikely to form if the DNS excitation energy is smaller than the magnitude of $B^*_{\rm fus}$. The more symmetric the entrance combination of nuclei, the higher the inner fusion barrier $B^*_{\rm fus}$, which the dinuclear system has to overcome on the way to the compound nucleus, and the lower the quasi-fission barrier $B_{\rm QF}$, hence QF offers stronger competition.

B. Competition between complete fusion and quasi-fission in SHE synthesis reactions

Nucleon transfer between the nuclei in a DNS has a statistic nature and there is a chance that the system may reach and overcome the B. G. point, and thus a compound nucleus will form. The alternative to that process will be the break-up of the system into two fragments (quasi-fission process). To calculate the probability of proton transfer from one nucleus to the other in a dinuclear system, we used an expression from work [32] and assumed that the macroscopic nucleon transfer probability P_z can be expressed in terms of the microscopic probability λ_z and level density ρ_z as $P_z = \lambda_z \cdot \rho_z$. The level density can be written in terms of the DNS potential energy as $\rho_z = \rho(E^* - U(Z, L))$, where E^* is the excitation energy of the double system. Finally, the proton capture P^+ and delivery P^- probabilities can be written as follows:

$$P^+ = \left\{1 + \exp\left[\frac{U(Z+1,L) - U(Z-1,L)}{2T}\right]\right\}^{-1}, \quad P^- = \left\{1 + \exp\left[\frac{U(Z-1,L) - U(Z+1,L)}{2T}\right]\right\}^{-1}, \qquad (8)$$

where $T = \sqrt{(E^*/a)}$ is the nucleus temperature; $a = 0.093A$ – the level density parameter. Knowing those relative ($P^+ + P^- = 1$) probabilities and using a random value uniformly distributed over the interval between 0 and 1, we randomly choose the direction for the DNS to move in: either the direction to the symmetric system or the direction to the compound nucleus, repeating this procedure as many times as needed to obtain the necessary statistics.

Fig. 11 shows the calculated results — the mass distribution of QF products for the reaction ^{48}Ca+^{208}Pb for $E^* = 33$ MeV. It is seen from that figure that the spectrum for the mass distribution of reaction fragments correlates with the structure of the driving potential. The maxima of the mass distribution are matched by the position of the local minima of the potential. This is a reflection of the nature of our approach to calculation in the case that there exist quasi-stationary states (local minima), which gives grounds to apply the statistical model.

C. Survival probability for the statistical decay of an excited compound nucleus

The formula for the cross-section after the process of de-excitation of fissioning excited compound nuclei can be written as follows:

$$\sigma_{ER}(E^*) \approx \pi\lambda^2 \sum_{l=0}^{l_{cr}} \sigma_{\rm CN}(E^*, l) \cdot W_{\rm sur}(E^*, l), \qquad (9)$$

where $\sigma_{\rm CN}$ is the production cross-section for the compound nucleus. There are a few approaches to calculate the survival factor $W_{\rm sur}$ for the compound nucleus in competition between the processes of fission and particle evaporation within the framework of the statistical model. This depends on the particular calculating algorithm used. For the decay of a heavy highly fissioning compound nucleus, the assumption that the main process competitive to the fission is neutron evaporation will be a good approximation to calculate the value $W_{\rm sur}$. In this case, there exists a simple phenomenological method for calculating the survival factor $W_{\rm sur}$, which can be written as the product of the ratios

$\langle\Gamma_n/\Gamma_{tot}\rangle = \langle\Gamma_n/(\Gamma_n+\Gamma_f\rangle \approx \langle\Gamma_n/\Gamma_f\rangle$ averaged over the evaporation cascade. The magnitude of the fissionability averaged over the evaporation cascade

$$\langle\Gamma_n/\Gamma_f\rangle = \left[\prod_{i=1}^{x}(\Gamma_n/\Gamma_f)\right]^{1/x}, \tag{10}$$

is derived from experimental cross-sections σ_{xn} with the help of equation (9). It depends weakly on the values E^* and x. Then the survivability of the heavy nucleus in terms of that approach can be written in the following analytical form:

$$W_{\rm sur}(E^*,l) \approx P_{xn}(E^*,l)\cdot\prod_{k=1}^{x}\left\langle\frac{\Gamma_n(E_k^*)}{\Gamma_f(E_k^*)}\right\rangle_k, \tag{11}$$

where x is the number of evaporated neutrons; P_{xn} – the probability of evaporating x neutrons; k – the index of the evaporation cascade stage.

In work [33], a large body of experimental data on few-neutron emission reactions was analysed, and semi-empirical systematics for the value $\langle\Gamma_n/\Gamma_f\rangle$ averaged over the cascade were obtained, which permitted describing the experimental data known by that time with an accuracy of up to the factor $2\div3$. The value P_{xn} in Eq.(11) was calculated following [34].

There exist other approaches to calculating the survivability of excited compound nuclei in the de-excitation process within the framework of the statistical model. Brief mention can be made of the latest calculations of that value for the considered compound nucleus of ^{256}No in works [35, 36]. In work [35], into the formula for calculating survivability

$$W_{\rm sur}(E^*) = \prod_{k=1}^{x}\left(\frac{\Gamma_n(E_k^*)}{\Gamma_{tot}(E_k^*)}\right)_k\cdot P_x(E^*) \tag{12}$$

the standard expressions were substituted from the statistical model for the probability of evaporating neutrons, protons, α-particles, γ-quanta and fission. A system of integrals inserted into one another (due to the number of stages in the evaporation cascade) was arrived at. Then numerical integration was carried out to calculate the magnitude of the survivability. Details can be found in the cited paper. In work [36], after a number of reasonable simplifications and integration, simple expressions were derived for the probability of evaporating neutrons and fission. The factor P_{xn} in formula (12) was calculated on the basis of Monte-Carlo method, simulating the probability of emitting neutrons of given energy. The neutron distribution over the energy e carried out of the excited compound nucleus was taken in both cited papers to be the Maxwellian distribution:

$$P_n(E^*,e) = C\sqrt{e}\exp\left(-\frac{e}{T(E^*)}\right) \tag{13}$$

In our case, we used the calculations of the $W_{\rm sur}$ value within the framework of a standard statistical model, which takes into account evaporation of not only neutrons but also of charged particles and γ-quanta. Since we study the decay of compound nuclei of considerable angular momentum, we made use of a quasi-classical version of the statistical model [37]. In that version, the probability of emitting particle ν(p, α, d, t, ^{3}He) of energy e_ν and angular momentum $\vec{l}$ in a unit time from a compound nucleus of angular momentum $\vec{L}$ and excitation energy E^* in the direction $\vec{n}$ is written as follows:

$$P_\nu(\vec{l},\vec{n},e_\nu) = (2s_\nu+1)\frac{\mu_\nu e_\nu}{\pi^2\hbar^3}\frac{\rho_d(E_d^*,L_d)}{\rho_m(E_m^*,L_m)}\cdot d\sigma_{\rm inv}(\vec{n},e_\nu) \tag{14}$$

where μ is the reduced mass of the system; s – the spin of the emitted particle; the symbols m and d indicate the mother and daughter nuclei, correspondingly.

Integrating the latter expression over the energy of the emitted particle gives the total probability and, thus, the partial width for emitting particles from the compound nucleus ($\Gamma_{n,\nu} = P_{n,\nu}/\hbar$). To calculate the partial width for emitting neutrons, charged particles (ν = p, α, d, t, ^{3}He), γ-quanta and fission, the following expressions were used

(see, for example, in reference [38]):

$$\Gamma_n(E^*,L) \approx \frac{(2s+1)\mu}{(\pi\hbar)^2\rho_m(U)} \int_0^{U-B_n} \sigma_{\rm inv}(e_n)\rho_d(U-B_n-e_n)e_n de_n,$$

$$\Gamma_\nu(E^*,L) = \frac{(2s_\nu+1)\cdot\mu_\nu}{\pi^2\hbar^3\rho_m(U)} \int_{v_\nu}^{U-B_\nu} \sigma_{\rm inv}(e_\nu)\cdot\rho_d(U-B_\nu-e_\nu)\cdot e_\nu de_\nu \quad (15)$$

$$\Gamma_\gamma(E^*,L) = \frac{3}{(\pi\hbar c)^3\rho_m(U)} \int_0^{U} \sigma_{\rm inv}(e_\gamma)\cdot\rho_d(U-e_\gamma)\cdot e_\gamma^2 de_\gamma$$

$$\Gamma_f(E^*,L) \approx (2\pi\rho_m(U))^{-1} \int_0^{U_s-B_f} \rho_s(U_s-B_f-\varepsilon)d\varepsilon,$$

where U is the heat energy of the mother nucleus. The cross-section of the reverse reaction $\sigma_{\rm inv}$, (reaction of the absorption of particles by the nucleus) was taken following work [39]. While calculating the partial width for γ-quantum emission, we only took account of emission of dipole γ-quanta. In this case, the inverse cross-section was taken in the form of a giant dipole resonance [40]. In the expression for the partial width of fission, the heat energy U_s and rotation energy E_r^s at the saddle point are related to each other by the relation $U_s = E^* - E_r^s$. While calculating Γ_f, account was taken of the fact that the rotation of the nucleus causes the fission barrier decrease: $B_f(L) = B_f(0) - (E_r - E_r^s)$. To calculate the level density, the known Fermi-gas expression (see, for example, [41]), was used

$$\rho(E^*) = \frac{\sqrt{\pi}}{12a^{1/4}(E^*-\delta)^{5/4}} \exp[S(E^*)], \quad (16)$$

In Eq. (16), the nucleus entropy S at the excitation energy E^* is taken to be described by the relationship $S = 2aT$, using the relation between the temperature and excitation energy of the nucleus $E^* = aT^2$; δ is the even-odd correction [41]. The level density parameter $a = \pi^2 g_0/6$ is expressed as a function of the one-particle density near Fermi's energy $g_0 = f(E_f) = const$. That the influence of shell effects in level density decreases as excitation energy increases was taken account of according to the phenomenological expression from [41]:

$$a(E^*) = \tilde{a}[1 + f(E^*)\Delta W/E^*], \quad (17)$$

Here $f(E^*) = 1 - exp(-\gamma\cdot E^*)$, ΔW is the shell correction to the nucleus mass; $\tilde{a}$ is the asymptotical magnitude of the level density parameter within the Fermi-gas model, which can be written in the general form as $\tilde{a} = A\cdot(\alpha+\beta A^n)$. Empirical values for the parameters $\alpha = 0.148$ MeV^{-1}; $\beta = -1.39\cdot10^{-4}$ MeV^{-1}; $\gamma = 0.061$ MeV^{-1} at $n = 1$ were found in work [42] from analysis of data on the level density with regard to the contribution of the collective states to the total level density.

To calculate $W_{\rm sur}$, the fission barrier for compound nuclei should be known. The fission barrier B_f is calculated as the sum of the liquid-drop component and the shell correction $\Delta W : B_f = B_f^{LD} + \Delta W$. For the compound nuclei of the heavy transfermium region, the liquid-drop component is a very small quantity.

In order to take into account the dependence of the shell correction on the excitation energy, we used the following formula: $B_f(E^*) = B_f^{LD} + \Delta W\cdot exp(-\gamma E^*)$. In our calculation, we used the value $B_f(E^*=0)$ from work [43].

D. Scheme of calculating the de-excitation process for an excited compound nucleus on the basis of the Monte-Carlo method

In this work, the de-excitation process for a nucleus was calculated by applying an approach based on simulating the random value — the Monte-Carlo method. Such an approach was successfully used to calculate the decay of heavy nuclei in [44]. In our opinion, it reflects the random, statistical nature of particle evaporation or fission in the most adequate way.

The angular momenta of the compound nuclei produced in a complete fusion reaction will be distributed over the value L, the vector $\vec{L}$ lying in the plane perpendicular to the ion beam. With the help of those random numbers, the

value of the angular momentum and its orientation in space were simulated. Then the maximum residual energies in the different channels of the statistical decay were simulated

$$E_\nu^{(\max)*} = E^* - E_{\rm rot} - B_\nu - V; \quad E_f^{(\max)*} = E^* - E_{\rm rot} - B_f \tag{18}$$

For all the $E_\nu^* > 0$, the type of emitted particle was also randomly chosen – $\nu = n, p, d,^3$He, α-particle or γ-quantum — on the basis of formulae (15). After the type of de-excitation process (the decay channel) was found, and if no fission occurred, the characteristics of the evaporated particles or γ-quanta were simulated. So their kinetic energy, carried-away orbital momentum and emittance angle θ were found. For a given type of particle, the magnitudes of $e_\nu, \vec{l}$ and $\cos\theta$ were simultaneously sampled using three random numbers, and then rejection was performed with the help of a fourth random number according to the three-dimensional probability density given by the expression [45]

$$W(e_\nu, l_\nu, \cos\theta) \sim l \cdot \exp\left[2\sqrt{a(E^* - E_\nu - (L^2 + l^2)/2J + Ll\cos\theta/J)}\right] \tag{19}$$

In a coordinate frame with a Z axis parallel to $\vec{L}$, the azimuthal angle of the vector $\vec{l}$ was simulated. The azimuthal angle of the escaped particle was simulated in a coordinate frame with a Z axis parallel to $\vec{l}$. The fission process was accounted for with the help of the weight functions $FU = \prod_{\nu=1}^{x} [1 - \Gamma_f/\Gamma_{tot}]$, which is especially convenient for highly fissioning nuclei and significantly saves computing time. All the values so found were brought to the centre-of-mass system of the colliding nuclei, and then the characteristics of the residual nucleus were calculated

$\vec{L}_d = \vec{L}_m - \vec{l}; \quad E_d = E_m - B_n - e_n - (L_d^2 - l^2)/2J; \quad A_d = A_m - A_n; \quad Z_d = Z_m - Z_n$

Then for that residual nucleus, the maximum residual energies were calculated for all the decay channels: particle emission, γ-quantum emission and fission. Among all the processes energetically allowed, the de-excitation of the nucleus was again simulated up to $E_s^* > 0$.

Presented in Fig. 12 are the calculated results for the probability of neutron evaporation from a nucleus of ^{256}No as a function of excitation energy. Also shown in the picture are the experimental values derived from the neutron evaporation cross-sections by the so-called pair reaction method (for details on the pair reaction method, see [46], from which that figure is borrowed). It is seen from the data presented in the figure, that for the larger excitation energy of the nucleus, it is necessary to take account of the shell correction being dependent on E^*. For $E^* > 40$ MeV, shell effects in such a heavy nucleus as ^{256}No damp out almost completely.

Shown in Fig. 13 are the calculated results for the survivability of an excited compound nucleus of ^{256}No obtained within the framework of the statistical model with three different approaches. The solid curve is the calculated result from this work. The dashed curve is the calculated result from work [35]. The dotted curve is borrowed from work [47], the model used being described in work [36]. It is seen from the figure that the different calculating methods give close magnitudes for fissionability in the region of excitation energies from 13 to 35 MeV, but as energy increases the magnitudes from the dotted curve begin to exceed the magnitudes from the other curves. This might be connected with the fact that the approach elaborated in [36] only takes account of the fission and neutron evaporation channels, whereas at the energies higher than 35 MeV, the channels with evaporation of charged particles begin to manifest themselves.

Summing up, in Fig. 5 we present a comparison both of the experimental capture cross-sections and of the excitation functions for evaporation of different numbers of neutrons measured in work [20] with our theoretical calculations. It is clearly visible that our approach adequately describes the measured data available for the reaction ^{48}Ca $+^{208}$Pb$\rightarrow^{256-xn}$No both on fusion and on the excitation function with particle evaporation.

V. ANALYSIS AND DISCUSSION

A. MED of fragments of the heated nucleus

In section III, we have shown that the MEDs of fragments are complex in structure and introduced the term *"quasi-fission shoulders"*. The introduction of that term was not incidental, and not only due to the fact that their characteristics differ from those of the classical fission. There was another reason for that. In works [48-50], the reactions ^{40}Ar $+^{208}$Pb and ^{50}Ti $+^{208}$Pb, which are close to our case, but involve lighter and heavier ions, were studied. It was shown that the angular distributions of fragments (ADF) for high mass/charge asymmetries, which exactly correspond to the "shoulders", have a pronounced forward-backward asymmetry. It indicates that the process is a non-equilibrium one [7, 8, 48-50]. At the same time, the ADFs for fragments of the mass/charge lying in the

vicinity of $A_{\rm CN}/2(Z_{\rm CN}/2)$ are symmetric about 90°. So, in our case the "shoulders" can be believed with good reason to be also of a quasi-fission nature.

In work [51], it was observed that the picture for the ADF in the reaction ^{40}Ar + ^{197}Au is similar to that in the reaction ^{40}Ar +^{208}Pb and shown that in both cases the ADF is representable as the sum of two components: a compound one and a quasi-fission one. To assess the partial cross-sections for reaction product yields, in works [52, 53] a similar procedure was also applied to the mass distributions of fragments in the reactions ^{208}Pb+^{50}Ti [5], ^{51}V+^{197}Au [52], and ^{197}Au+^{63}Cu [53]. In recent work [54], it was also shown for the reaction ^{48}Ca+^{168}Er that experimentally observed MEDs of fragments are the sum of classical fission and quasi-fission components. In present work we will follow this way while analysing the MEDs of fragments as well and show its validity.

1. Symmetric fission properties

For the nuclei of the second half of the periodic table, the properties of classical symmetric fission, characteristic of heated nuclei, are quite well studied for reactions with heavy ions and known from numerous both experimental [5, 7, 8, 18, 19, 23, 24, 55-63] and theoretical [21, 22, 64-68] works. Their MD of fragments is a one-humped gaussian-like curve, whose variance, σ^2_M, increases approximately in proportion to the increasing temperature of a fissioning nucleus: $\sigma^2_M \sim T$ and also $\sigma^2_{\rm TKE} \sim T$, whereas $\langle TKE\rangle$ is practically independent of E^* (or T). Experiments showed that an increase in the angular momentum l of a fissioning nucleus results in an additional increase in the σ^2_M for heavy nuclei with $Z^2/A > 30$ [18, 55, 58, 63] and in a decrease in the σ^2_M for light nuclei with $Z^2/A < 30$ [59, 61, 68]. In review [24], the properties of the MEDs of fragments for heated nuclei with $A_{\rm CN} > 100$ were analysed and systematised. In works [18, 24, 63], in studying the fission of the superheavy compound nucleus of ^{260}Rf ($Z = 104$) produced in various reactions: ^{16}O + ^{244}Cm, ^{20}Ne+^{240}Pu, ^{24}Mg+^{236}U it was found that the properties the MEDs of fragments — a rise in σ^2_M and $\sigma^2_{\rm TKE}$with the increasing T and l, the independence of $\langle TKE\rangle$ of those variables - fit in with the known picture of classical fission.

To find the characteristics of MEDs for the symmetric fission of ^{256}No (Figs. 7 and 8), we approximated the MD of fragments with a gaussian G. On the left-hand side of Fig. 14, the mass distributions of fragments, depicted on a logarithmic scale, are given in relation to the parameter $(M - A/2)^2$. Being so represented, the gaussian is a linear function. In Fig. 14 it is quite clearly visible that at the parameter value $(M - 128)^2 \cong 800 - 900 (M_L \cong 100)$, the experimental points start to deviate upwards from G, which adequately approximates the beginning part of the MD. In the central panels of Fig. 14, the G approximation for the MD is shown on a linear scale. In Table I, given are the values of the variances of the gaussian distributions (σ^2_M) for five magnitudes of ^{48}Ca ion energy. On the right-hand side of Fig. 14, shown are (only for light fragments) the "quasi-fission shoulders" derived in a "pure" state by subtracting the G-function from the experimental yield of fragments:

$$Y_{\rm QF}(M) = Y_{\rm exp}(M) - Y_{\rm G}(M). \tag{20}$$

Let us consider the properties of the MED for symmetric fission, or more precisely, the experimental dependences of $(\sigma^2_M)_G, \langle TKE\rangle, \sigma^2_{\rm TKE}$ on T and l. In Fig. 15, the dependence is shown of those characteristics on the nucleus temperature at the scission point $T_{\rm sc}$, which we find, as in a great number of works (for example [24, 63,69] from

$$T_{\rm sc} = (E_{\rm sc}/\tilde{a})^{1/2}, \quad E_{\rm sc} = E^*_{LD} + Q_f - \langle TKE\rangle - \langle\nu_{\rm pre}\rangle\langle E_\nu\rangle - E^{\rm sc}_{\rm rot} - E_{\rm def} + E_{\rm diss}, \tag{21}$$

$$E^*_{\rm LD} = E_{\rm CM} + (\Delta M_i + \Delta M_t - \Delta M^{\rm LD}_{\rm CN}), \tag{22}$$

where $E^*_{\rm LD}$ is the nucleus excitation energy measured from the ground state of the liquid-drop model ; ΔM_i and ΔM_t the experimental magnitudes of the mass defects for the nuclei; $\Delta M^{\rm LD}_{\rm CN}$ the liquid-drop magnitude of the mass defect for the compound nucleus of ^{256}No from work [70]. $\tilde{a} = 0.093A_{\rm CN}$ is the level density parameter [41,71]. Q_f is the reaction energy for the symmetric scission of the nucleus into fragments. $\langle TKE\rangle$ is the measured average magnitude of the TKE. $\langle\nu_{pre}\rangle\langle E_\nu\rangle$ is the average energy carried away by the pre-fission neutrons calculated as proposed in [15]. The value of $\langle\nu_{pre}\rangle$ is found from systematics [24] and given in Table I for all the magnitudes of ^{48}Ca-ions energy. $E^{\rm sc}_{\rm rot}$ is the nucleus rotation energy at the scission point. $E_{\rm def}$ is the energy spent on deforming the fragments. $E_{\rm diss}$ is the energy dissipated from the collective degrees of freedom into one-particle degrees of freedom.

Let us explain some components in expression Eq. (21). The nucleus rotation energy at the scission point was found from expression from Ref. [55]

$$E^{\rm sc}_{\rm rot} = l^2\hbar^2/2J^{\rm sc}_\perp + T_{\rm sc}/2, \tag{23}$$

where $J_{\perp}^{\rm sc}$ is the nucleus moment of inertia relative to the axis perpendicular to the fission axis. In the end, the matter comes to finding $J_{\perp}^{\rm sc}$. The LDM by Strutinski [72] defines a location where scission occurs as a critical point associated with a loss of stability against breakup into two fragments and uses J_0 units for $J_{\perp}^{\rm sc}$ (J_0 is the rigid body moment of inertia of the spherical nucleus). For the nucleus of ^{256}No, $J_{\perp}^{\rm sc} \cong 4.3 J_0$. Hence it follows that

$$E_{\rm rot}^{\rm sc} \cong E_{\rm rot}^{0}/4,3 + T_{\rm sc}/2. \tag{24}$$

From the classical rotating liquid-drop model [73], it is known that

$$E_{\rm rot}^{0} = 34,540(l^2/A^{5/3}) \tag{25}$$

It should be noted that in the framework of LDM [72], the scission point has by no means non-zero neck thickness. Scission occurs when the neck is thick enough, the common elongation not changing. So scission does not result from the neck gradually thinning with the increasing deformation of a fissioning nucleus, as is often assumed in a lot of works.

That is, a breakup is by no means preceded by a gradual decrease in the neck thickness accompanied by an increase in the deformation of the fissioning nucleus, contrary to what is frequently assumed in a lot of works. Such theoretical definition of the scission point is supported by the analysis of various characteristics of measured energy distributions of fragments when taking into account viscosity of nuclear matter [24, 74-76].

As for the parameters $E_{\rm def}$ and $E_{\rm diss}$ in expression (21), it can be said that there is currently no general agreement on those values — they are dependent on the model used, the nature and magnitude of nuclear viscosity (two-body or one-body viscosity). But account should be taken of the fact that $E_{\rm def}$ and $E_{\rm diss}$ compensate each other to some extent. Therefore, following works [24, 63, 77], we took $E_{\rm def} = 0$ and $E_{\rm diss} = 0$. The temperature $T_{\rm sc}$ found according to Eq. (21) is given in Table I. It should be noted that $T_{\rm sc}$ rises very slowly in those cases at the high energy of bombarding ions when $\nu_{\rm pre}$ are evaporated. That property of fissioning heavy nuclei, noticed in works [18, 24, 77], results in the fact that reaching the scission point, the nucleus heats up only slightly in spite of the increasing energy of the ions.

In Fig. 15(a), it is clearly visible that within the limits of experimental error, the magnitudes of $\langle TKE \rangle$ are independent of $T_{\rm sc}$ (excitation), which is characteristic of the fission of heavy and superheavy nuclei. For $T_{\rm sc} \geq$ 1.83 MeV, the varience $\sigma_{\rm TKE}^2$ (Fig. 15(b) increases proportionally to $T_{\rm sc}$. The shaded magnitudes of $\sigma_{\rm TKE}^2$ belong in the region peculiar to classical fission. That region was determined in works [18, 23, 24, 63] for the fission of the heavy nuclei produced in reactions with "light" heavy ions ($A_i < 26$) with taking into account an increase of $\sigma_{\rm TKE}^2$ with l. For the temperature $T_{\rm sc} \leq 1.82$, there is no decrease in the magnitude of $\sigma_{\rm TKE}^2$, and at $T_{\rm sc} = 1.75$ ($E_{\rm lab} = 211$ MeV), whereas the magnitude of $\sigma_{\rm TKE}^2$ even grows. As has been noted in section III, this points to the influence of shell effects on the MED of fragments for the sufficiently low-energy fission of ^{256}No.

In Fig. 15(c), the variance of fragment masses $(\sigma_M^2)_G$ is shown as a function of $T_{\rm sc}$ for the five largest magnitudes of the energy of ^{48}Ca ions (Figs. 6, 7, 14). The cross-hatched region of the $(\sigma_M^2)_G$ magnitudes, as in Fig. 15(b), belong in the region typical of normal fission. Since $T_{\rm sc}$ increases only slightly with increasing ion energy, then, as shown in works [18, 24, 63], the increase in $(\sigma_M^2)_G$ is to a large degree connected with the increase in the angular momentum l of the fissioning nucleus, and $(\sigma_M^2)_G \sim \langle l^2 \rangle$. Therefore for the temperature $T_{\rm sc} = 1.93$ MeV ($E_{\rm lab} = 242$ MeV), the variance $(\sigma_M^2)_G$ shows a sharp enough rise. That increase in variance lies within the boundaries of what can be expected for normal fission.

So we come to the conclusion that the characteristics of the MEDs of fragments for the fission of ^{256}No for the region of symmetric masses fit in with ordinary classical fission.

2. Properties of the quasi-fission process

In contrast to the properties of classical fusion-fission, the characteristics of quasi-fission process depending on the nucleon composition, excitation energy and entrance channel energy have been poorly studied. First of all, it is true for the energy characteristics of QF. Early it was believed, that TKE for the QF process did not differ from that for the FF process. However, on analysing a great number of reactions induced by various ions, it has been shown recently in work [24] that for QF, the TKE of fragments is on average larger. *Experimental* dependences $TKE_{\rm QF}(M)$ and $\sigma_{\rm TKE(QF)}^2(M)$ were not practically considered. Just quite recently, it has been shown in work [54] that in the reaction ^{48}Ca+^{168}Er→^{216}Ra at $E^* = 40$ MeV, about 30% of the fragments are associated with quasi-fission and have TKE higher than the TKE of the fragments produced in a classical FF process and that this experimental fact, by analogy with low-energy fission, can be accounted for by QF being strongly influenced by shell effects. Besides, it has been demonstrated in [54] that the properties of the MED of fragments for ^{216}Ra formally satisfy the standard

hypothesis about independent fission modes [55, 78, 79]; in that case, there are just QF and normal FF. Our version of the DNS model corresponds to this concept: FF and QF are assumed to be competitive processes and the MED of fragments for a process is considered not to be influenced by the other process.

From Fig. 7, it is seen that the fragment masses in the region of the quasi-fission shoulders have TKE higher than that expected for a FF process, which agrees with work [54]. Therefore in this case the MED is also decomposable into components, and this can be done in accordance with Eq. (20) and an expression from [54]:

$$TKE_{\rm QF} = [TKE_{\rm exp} - TKE_{\rm FF}(Y_{\rm FF}/Y_{\rm exp})]/(Y_{\rm QF}/Y_{\rm exp}) \tag{26}$$

Here everywhere M-dependence is meant.

The decomposition was done for the energy $E_{\rm lab} = 230$ MeV, for which the data were statistically sufficient to the largest degree. The experimental dependence $\langle TKE\rangle(M)$ in Fig. 7 was fitted with a parabolic curve [55].

$$TKE(M) = TKE(A/2)(1-\eta^2)(1+\rho\eta^2), \quad \eta = (M-A/2)/(A/2), \tag{27}$$

where ρ is an empirical parameter that defines the extent to which the width of this parabolic curve deviates from the predictions of LDM [21], for which $\rho = 0$. In our case $\rho = 0.25$, which is in good agreement with the results obtained for classical fission [55].

The mass distribution of light QF fragments is presented at the right of Fig. 14 for four values of energy. Fig. 16 shows the decomposed MED of light fragments for the energy $E_{\rm lab} = 230$ MeV. Shown in Figs. 16(a) and 16(b) are the mass distribution for QF and the dependence $\langle TKE\rangle(M)$ respectively. It is clearly seen that the $TKE_{\rm QF}(M)$ is higher by $7-15$ MeV than $TKE_{\rm FF}(M)$ and that on the whole it is also parabolic in form, which is also a formal similarity to the modes of classical low energy fission [80]. However the width of the parabolic dependence $TKE_{\rm QF}(M)$ is greater than $TKE_{\rm FF}(M)$ (parameter $\rho = 0.6$).

It would appear natural to hypothesize, as in [54], that the properties of the MED for QF can be accounted for by shell effects, which is also predicted by our version of the DNS model. In Fig. 16(a), the mass number of the closed spherical shells $Z = 28, N = 50$ are indicated with arrows. They were calculated on the basis of the simple assumption that charge is proportional to mass (unchanged charge density). In this case, only a light "quasi-fission shoulder" is associated with closed shells. The complementary heavy fragment belongs to the mass region $M \sim 160-190$ and is non-spherical. The influence of shells with $Z = 50$ and $N = 82$ near the mass $M = A/2$ will be considered in the next section.

The properties of QF similar to those discussed, with a maximum yield of fragments at $Z_{L(QF)} \sim 28$ and $M_{L(QF)} \sim 75-85$, have already been revealed in the reactions ^{51}V+^{197}Au and ^{197}Au+^{63}Cu in works [52, 53] respectively. The effects under discussion seem to manifest themselves in the mass region of quasi-fission fragments $M \sim 70-85$ in the reactions ^{58}Ni+^{124}Sn [81], ^{124,136}Xe+^{58,64}Ni [82], ^{208}Pb+^{50}Ti,^{64}Ni [5], ^{40}Ar+^{208}Pb [83] as well as at the forward angles in the reaction ^{64}Ni+^{197}Au [84]. There arises an interesting situation with the ^{48}Ca+^{168}Er reaction [54]. In this case, the complementary heavy fragment, its mass $M_H(QF) \approx 130-140$, is close to the magic spherical shells with $Z = 50$, $N = 82$ in nucleon composition, therefore, unlike the case discussed, both the light fragment and the heavy fragment are represented in the quasi-fission shoulders, which results in more pronounced QF. The same is probably true for the ^{164}Ho+^{58}Ni reaction [85], characterized by maxima just in the same fragment mass regions at the forward and backward angles peculiar to QF. At the same time, at the angles close to 90° in the vicinity of the mass $M \sim A/2$, as in our measurements, a symmetric near-Gaussian component, which we as well as the authors of [55, 85] believe to be associated with FF, is clearly visible.

From this point of view, the reaction ^{40}Ar+^{208}Pb $\rightarrow^{248}$Fm at $E_{\rm lab} = 247$, discussed in work [83], is very interesting. This reaction is close to the reaction under consideration, and its MDs show clearly defined quasi-fission shoulders. This feature has somewhat escaped attention before. However in our opinion the results of work [83] are of outstanding importance in understanding the properties of QF. In this work, the MDs of fission fragments for ^{248}Fm were measured for two angles: $-24°$ and $-46°$. Having analyzed those data, we extracted the QF component from the total yield of fragments. The results obtained are presented in Fig. 17, at the left of which the MD of fragments is shown for forward angle registration. The quasi-fission shoulder is perfectly well visible. That this shoulder is associated with quasi-fission rather than with an exotic classical fission mode, follows from work [48], already cited. In this work, it was shown that the angular distributions of the fragments from the shoulders are highly asymmetric; whereas in the region of symmetric charges/masses, the angular fragment distributions fall into the pattern of normal fission. The central symmetric peak in Fig. 17, associated with a FF process, can be approximated, as in the case under discussion, by a Gaussian to a good accuracy. The extracted QF component, indicated with open circles, does not merge with the quasi-elastic peak as in the case of ^{48}Ca-projectiles and is distinctly limited on both the light and heavy fragment mass sides; and again the quasi-fission shoulder is composed of fragments with near-magic numbers close to $Z \approx 28$ and $N \approx 50$. At the right of Fig. 17, the MD of fragments is shown for the same nucleus but for a larger angle of measurement. In this case, the quasi-fission shoulders are less prominent but the lower portion of the MD is clearly

seen to be wider, in the same way as in the case under discussion at the energy of ^{48}Ca ions $E_{\rm lab} = 242$ MeV. The QF is characterized by the same mass range of light fragments as that shown at the left of Fig. 17. Unfortunately, work [83] does not discuss the energy distributions for this particular reaction. It is noteworthy that the ^{248}Fm compound nucleus has the initial excitation energy $E^* \cong 78$ MeV and that the number of pre-fission neutrons in the quasi-fission shoulders region is only 1.2 [83]. Thus, although E^* is high enough, the conclusion can be drawn that shell effects play a greater role in QF than in classical FF, which we have already shown in work [54] for ^{216}Ra.

It should be recalled that although the role of shell effects in QF has been discussed for a long time [6, 86-88], the interaction of massive ions with actinide targets (or U ions in reactions of inverse kinematics) is basically studied. The MDs of fragments of such reactions are characterized by the presence of doubly magic lead, $M_H \sim 208$ ($Z_H \sim 82, N_H \sim 126$), which is variously accounted for. For example, the authors of works [6, 87], studying the reactions ^{40}Ar, ^{48}Ca+^{238}U, reasoned that the peak associated with lead is due to the further sequential fission of fragments with mass $M_H = 215 - 230$; whereas the authors of work [88] hold to the idea that this peak owes its existence to strong lead shells nevertheless. To return in our case to the reaction ^{48}Ca +^{208}Pb at $E^* = 33$ MeV, it is unlikely for fragments of any mass number to undergo sequential fission [41, 71]. On the contrary, increased yield of fragments with mass $M = 60 - 80$ is observed, their TKE being higher compared to the TKE expected for a FF process.

Recently, studying the reactions ^{48}Ca+^{238}U, ^{244}Pu, ^{248}Cm at $E^* \sim 30$ MeV [16, 89, 90], we have found corroboration of the fact that the properties of the QF of superheavy nuclei are influenced by magic shells, both the shell structure of heavy fragments (nuclei close to ^{208}Pb) and light fragments (nuclei close to ^{78}Ni) being of importance, which is shown in [54] as well. So, based on the results of the experiment discussed and previous research, we can conclude that in QF, closed spherical shells play an important role and that shell effects damp out much differently than in known and usual classical fission. The questions immediately arise "Why so?" and "Why is all this possible?".

We believe that the answers, at least qualitative ones, can be provided by our model, based on the DNS concept, and models [91-93], conceptually close to it. In Fig. 10, as have already been mentioned in section IV A, the potential energy of the DNS is shown as a function of the mass of the light fragments produced in a QF process. Heavily indented due to the shell effects, the potential energy has three global minima: at $M_L = 48, 82$ and 126, the complementary heavy fragments being of $M_H = 208, 174$ and 130 respectively. The first numbers of those two series are easy to interpret: they are associated with doubly magic the ^{48}Ca projectile and the ^{298}Pb target. The second and shallower minimum is associated with ^{82}Ge ($Z = 32, N = 50$); in this case the fragment charge is close to the magic number $Z = 28$ and the neutron number is exactly equal to a magic neutron number, the complementary heavy fragment being of a non-magic number. The third and deeper minimum is due to the fact that both fragments are close to magic Sn.

At the bottom of Fig. 11, the mass distribution of QF products is shown; it was calculated in the way described in section IV B. It reflects completely the structure of the DNS potential energy. The first peak, at $M_L \approx 48$, can in no way be distinguished in experiment from the peak associated with deep inelastic transfer reactions, which is in fact seen in Figs. 6 , 7 and 8. The second peak with average mass $M_L \approx 82$ is associated with the quasi-fission shoulder, which was found experimentally. The third peak in Fig. 11, at mass $\sim A/2$, is characterized by a yield that is three orders of magnitude smaller than that at mass $M_L \approx 82$. Although that peak is associated with the deepest minimum of the potential energy it will be practically impossible to observe this peak in experiment because the yield of FF is predominant. This minimum of the DNS potential energy is populated slightly, which is accounted for by the fact that the probability of the DNS breaking up before reaching a symmetric configuration is high. The total capture-fission cross-section σ_c in Fig. 5 (indicated with a solid line) was calculated taking account of both the FF cross-section $\sigma_{\rm FF}$ and the whole sum of the mass yields associated with QF (this sum is shown in Fig. 11), the peak at $M_L \approx 48$, which is responsible for a major part of the calculated QF cross-section, being taken account of as well. To consider the experimental MD, the contribution of QF to the total MD is $15 - 20\%$ for the operating angular range of our spectroscope on condition that only fission-like events are taken into account, as shown in Fig. 7.

In our model as well as in models from [91, 92], the DNS excitation energy is counted from the DNS potential energy for each mass instead of the CN ground state. That is why the excitation energy of fission fragments, for example with $M = 82$, will be by about 20 MeV lower than E^* of the compound nucleus, since it is exactly this value by which the potential energy for this mass is "lifted" over the CN ground state. Thus, the fission fragment having this mass formed in the reaction ^{48}Ca+^{208}Pb will be more cold than that formed in the FF process.

In Fig. 18(a), the relative mass yields of light fragments for QF obtained experimentally and calculated by our model are compared. It is clearly visible that the experimental distribution is far wider than that predicted theoretically and that in this case it lacks a clearly defined peak-like shape, while, as seen from data on the fission of ^{248}Fm (Fig. 17), the experimental quasi-fission component is really peak-like in shape. That the theoretical and experimental distributions for QF differ in width is most likely to be connected to the fact that a statistical approach has limited application in calculating such a QF characteristic as MD, since according to works [5, 7, 8] the formation of fragment mass in QF is a dynamical process with the mass relaxation time $\tau = 5.3 \times 10^{-21}$ c [8]. Therefore our statistical calculations can

be considered as a first approximation that only predicts QF characteristics in a qualitative way.

In recent work [92] a dynamical transport model of QF has been developed on the basis of the DNS concept. In this model, which takes account of shell effects, a change in the mass (charge) asymmetry of DNS is a result of diffusion. Fig. 18(b) shows the experimental and calculated [92] relative yields associated with QF for the reaction concerned. As can be seen from that figure, the MD for QF calculated in the framework of this model is a distribution that smoothly rolls off to become symmetric and resembles the experimental distribution, there being minor peculiarities due to the shell effects discussed above. This MD is far wider than that that we found. In model [92], the QF process has a characteristic time of $30 - 40(\times 10^{-21})$ s, which is $3 - 8$ times larger than that found in experiment [7, 8]. Such a time is typical of the classical fission of heavy nuclei [22, 66, 67, 77, 83], and the angular distribution for each mass will be symmetric about 90°, which contradicts experimental data [7, 8, 48-51].

As a result, we can conclude that on the whole both our model of DNS and the model from work [92] provide qualitatively correct predictions about some properties of QF however these models need improving for them to be capable of making quantitative predictions about the characteristics of QF. The theoretical approach realized in work [93] seems, in our opinion, promising. At present, this approach, which takes account of shell effects, is the most consistent in treating the fusion and quasi-fission of heavy nuclei in reactions with massive ions.

B. Properties of low-energy fission

1. Analysis of experimental results

It is now common knowledge that for spontaneous fission, the MEDs of fragments for the superheavy nuclei beginning with ^{258}Fm are bimodal in structure [19, 94-97]. Typical for those nuclei are "anomalously" narrow symmetric MDs with the high total kinetic energy of fragments of up to ~ 235 MeV. At the same time, the MD of those nuclei has a component of much larger width but with the lower of $TKE \sim 200$ MeV, which corresponds to the standard fission of those nuclei. The ratio of the high-energy to the low-energy component (mode) significantly varies with the nucleon composition, but the universal tendency is that for Z fixed, there is a sharp increase in the yield of the symmetric mode with high TKE (see the systematics of mass yields and TKE distributions in works [96, 97]) as the neutron number of both fragments approaches the $N = 82$ neutron shell. To compare, for example, the MDs for chains of Fm and No isotopes in spontaneous fission, the standard two-humped distribution transforms drastically to the clearly defined narrow symmetric distribution as the neutron number of a fissioning nucleus changes from 157 to 158 in the former case and from 154 to 156 in the latter case in spite of the fact that in the TKE distributions, the high-energy mode is dominant in the case of ^{258}Fm and the low-energy mode in the case of ^{258}No [94, 95].

The properties of the MDs of fragments of the nuclei under discussion can change rather drastically, for example, from an asymmetric distribution, in the case of ^{256}Fm(s, f) [97-99], in which the nucleus is not excited, to a symmetric distribution, in the reaction $^{255}\mathrm{Fm}(n_{\mathrm{th}}, f)$, the excitation $E^* = 6.4$ MeV [98,100], or from a very narrow symmetric distribution to a distribution also symmetric but several times larger in width, as in the case of ^{258}Fm(s,f) [94] and $^{257}\mathrm{Fm}(\mathrm{n_{th}}$, f) [101, 102]. At the intermediate excitation ($E^* = 10 - 20$ MeV), the shell effects begin to damp out, but not to such a degree that the modal structure be unobservable. For superheavy nuclei, this is most clearly demonstrated in work [98], in which it is shown that for the already discussed ^{256}Fm nucleus, the high-energetic mode appears in the thermal-neutron-induced fission of ^{256}Fm whereas it is absent in the spontaneous fission of ^{256}Fm. Its further behaviour is traced up to $E^* = 17.5$ MeV, at which it also manifests itself, but not so clearly.

Recently, it was shown in our work [19] that bimodality is also exhibited by the nucleus of ^{270}Sg ($Z = 106$) excited up to $E^* = 28$ MeV. However, it should be noted that this is a unique case since the breakup into exactly equal parts results in fragments with the magic neutron number $N = 82$.

Theoretical calculations [103-111] made for superheavy nuclei showed that on the potential energy surface in the multidimensional deformation space of fissioning nuclei, there exist at least two [104, 105, 108-111] or even three [103, 106, 107] fission valleys for that process to follow. One of the valleys, named Super-Short by Brosa et al. (SS) [103, 104], enables those nuclei to have near-magic numbers of neutrons and protons of $N \sim 82$, $Z \sim 50$ in both fragments. For superheavy nuclei, the SS valley was found in calculations [105, 108] to persist up to ^{270,272}Hs ($Z = 108$) and even up to $^{278}110$ [104] and $^{290}110$ [106].

Now let us consider the properties of the MEDs for low-energy fission of ^{256}No. Fig. 19 presents the total (Fig. 19(a)) and differential distributions of fragment masses for $TKE > 201$ MeV(Fig. 19(b)) and $TKE < 201$ MeV(Fig. 19(c)) at the lowest energy $E_{\mathrm{lab}} = 211$ MeV ($E^* = 17.6$ MeV). For the high TKE, it is clearly visible that the MDs are two-humped in structure in the region of the mass of heavy fragments $M_H \cong 131 - 135$, which is characteristic of the high TKE in the fission of all actinides. For superheavy nuclei, the shape of the distribution very much resembles the MDs of fragments in the spontaneous fission of ^{259}Lr ($Z = 103$) [112]. For the low $TKE < 201$ MeV, seen in Fig. 19(c) is a wide and flat distribution held by the masses $M_H \cong 140 - 150$. Such shape of the MD low-energy

component is also typical of the fission of superheavy nuclei; for example, the spontaneous fission of ^{259}Md [94] or ^{260}Md [113], in which the low-energy component even has a slight valley for the symmetric masses. Thus, we see that at $E^* = 17.6$ MeV, the MD of fragments for ^{256}No consists of two components at least.

Let us consider the energy distributions (EDs) of fragments for ^{256}No. Presented at the left of Fig. 20 are the distributions TKE for four values of the energy of ^{48}Ca-projectiles. For the two lowest energies, attention is attracted by the fact that the bottom of the distributions is larger in width. Shown at the right of Fig. 20 are the EDs of fragments for the same energies of ^{48}Ca ions, but only for the symmetric masses in the range $M = 124 - 132$, that is, for those masses where a two-humped MD is experimentally observed (Fig. 19). For the largest energies $E_{\rm lab} = 242$ and 225 MeV, those distributions are practically not different from the total distributions in any way. But for the two smallest energies, especially for $E_{\rm lab} = 211$ MeV ($E^* = 17.6$ MeV), two TKE components are distinctly visible. One of them is a dominant low-energy component with $\langle TKE\rangle_{\rm low} \sim 200$ MeV, and the other is a high-energy one with a $\langle TKE\rangle_{\rm high} \sim 233$ MeV. Those $TKEs$ as well as the mass yields are characteristic respectively of the standard and the SS mode in the spontaneous fission of superheavy nuclei [94-97]. So, the experiment shows the fission of excited ^{256}No to be bimodal, as demonstrated both by the MD and ED, though the contribution of the SS mode on the whole is slight.

We will point out especially that we think the SS mode to be inherent in the classical low energy fission of ^{256}No, though, as discussed above, from the theoretical standpoint such fragments may be produced in quasi-fusion as well, their yield being smaller as compared with fragments of $M = 60 - 90$ (Figs. 11 and 18). However, to return to Fig. 8, in which the two-dimensional matrix ($M - TKE$) for $E_{\rm lab} = 211$ MeV is given, the matrix only has isolated events for the region of M and TKE essential to the quasi-fission shoulders. So there should be no QF events associated with masses $M = 120 - 135$ at all and our assumption that the SS mode occurs in a classical FF process is, in our opinion, irrefutable.

Now let's return to Fig. 7 from which it can be seen that the dependence $\sigma^2_{\rm TKE}(M)$ has a clearly noticeable small yet statistically important peak in the symmetric region. An irregularity in the dependence $\sigma^2_{\rm TKE}(M)$ always indicates that in the mass region in which this irregularity is observed, the MED of fragments is of complex structure. To account for this fact, the fragment yields as a function of TKE for the total mass region and different mass ranges are shown in Fig. 21. It can be seen that in the distributions for the total mass region and for the symmetric mass range $M = 124 - 132$, there is a high energy component similar to that at an energy of 211 MeV but with a smaller yield. This component becomes noticeable at very high $TKE > 245$ MeV because it is covered by the main dome curve of symmetric fission. Nothing of the kind is observed for the other mass ranges.

Fig. 22 shows the MDs of fragments for various high energy ranges of TKE. For the ranges of $TKE = 211 - 221$ MeV and $221 - 231$ MeV, the MDs are near-Gaussian in shape though their peaks are seen to be narrow. For the highest $TKE > 241$ and 245, a two-humped MD is seen with a peak due to the heavy fragment of $M = 132$, there being obviously two components: a two-humped narrow component and a wide pediment-like component. So at $E^* = 33$ MeV, as at $E^* = 17.6$ MeV, the SS fission mode is seen, but its contribution to the total distribution is small. At those values of E^*, the low-energy mode is already close to the liquid-drop mode in properties.

Let us make a qualitative analysis of the picture obtained. To follow the traditional assumption that the charge of a fragment is proportional to its mass, for the region $M_H \cong 131 - 135$ its charge will be $Z_H = 52 - 54$, the neutron number being $N_H = 79 - 81$. That is, the Z of the heavy fragment is close to a magic number ($Z = 50$), but slightly larger than it, and the neutron number is also a near-magic number ($N = 82$), but slightly smaller than it. For the complementary light fragment, the yield peak lies in the mass region $M_L = 121 - 125$; if so, its charge will be $Z_L = 48 - 50$, and $N_L = 73 - 75$. Then the light fragment has charge close to magic charge and a neutron number far smaller than a magic number. So the SS mode is due to the proximity of the nucleon composition both by N and by Z to a magic number for the heavy fragment and only by Z for the light. Since the total number of neutrons is nevertheless not enough to close the spherical shells in both fragments, this mode is not dominant for ^{256}No and manifests itself only slightly.

According to various theoretical estimates [114-116], the fission barrier for cold ^{256}No $E_f = 6.4 - 8$ MeV. In recent experimental [117] and theoretical [118] works, it has been demonstrated that ^{254}No produced in a ^{208}Pb (^{48}Ca, $2n$) reaction has a fission barrier $E_f > 5$ MeV for a nuclear spin of $12\hbar$ till $22\hbar$. Therefore in our case the excitation energy at the saddle point will be $E_{\rm sp} = 10 - 12$ MeV for $E_{\rm lab} = 211$ MeV and $E_{\rm sp} = 22 - 24$ MeV for $E_{\rm lab} = 230$ MeV with taking into account 0.3 pre-scission neutrons. This is rather low excitation, and shell effects, responsible for the production of fission valleys, certain to play a key role in the formation of the MEDs of fragments, which reflects on their structural peculiarities in Fig. 19-22.

2. Theoretical calculations

The theoretical calculations of the ^{256}No potential energy landscape in relation to the distance between the centeres of the future fragments and their elongations are presented in work [105]. On that landscape, an SS-valley is clearly visible. The valleys ramify into a standard valley and the SS-valley from the second minimum, but the external potential barrier in the SS-valley is higher than that in the standard valley, and it is more advantageous for a nucleus, while fissioning, to overcome the traditional standard barrier, whose penetrability is higher than that of the barrier in the SS-valley. Therefore the SS-mode is practically unobservable in spontaneous fission [95, 97, 119]. In induced fission, as excitation energy increases, firstly, the values of barriers decrease in magnitude [120] (shell effects damp out); secondly, the potential energy landscape gets smoother [120], which decreases the difference in the heights of the barriers in the different valleys; thirdly, excitation of the nucleus allows an SS-valley of higher energy to be populated, though with lower probability than a standard valley.

This phenomenon, i.e the manifestation of some mode which was not observed in the spontaneous or near-barrier fission and its appearance at a certain excitation of the nucleus, has been already observed for different nuclei. In works [55, 121] for ^{213}At the appearance of the standard symmetric mode was observed against the background of the dominant symmetric mode. In [122, 123] for the region of heavy isotopes Ra-Ac, on the contrary, the appearance of the symmetric mode was observed at a dominance of the standard mode; in [98, 100] for ^{256}Fm, already mentioned, the appearance of the SS mode was observed at a dominance of the standard mode. All those data, as with ^{256}No, can only be accounted for in terms of independent fission modes arising from the fact that there are valleys on the surface of the potential energy in the multidimensional deformation space of the fissioning nucleus.

In this paper we present new multi-parametric calculations of the ^{256}No potential energy near the scission point as a function of mass asymmetry. The calculations were made with the use of the Strutinsky shell correction method. The surface of the nucleus was described in parametrization based on Cassinian ovals [107], where parameter α characterizes the nucleus elongation and parameter α_3 and others odd number parameters describe the asymmetry of the figure. Deformations of a higher order of up to α_{31} were taken into account in the process of minimization.

Figure 23 shows the potential (deformation) energy of ^{256}No near the scission point at the fixed neck radius $R_{\rm neck} = 0.3R_0$ (R_0 is the radius of the spherical nucleus of the same volume). The neck radius is close to the critical one as the fissioning nucleus goes over from the fission valley to that of the separated fragment [124]. The calculations have shown that the process of fission near the scission point evolves in four more or less independent valleys, indicated by letters A, B, C and D in Fig. 23. It looks like the valleys A, C and D intersect in the considered coordinates. This happens because of the multidimensionality of our calculations, i.e. the valleys lying in the area of intersection are characterized by different deformations of a higher order and are separated by the potential barriers. It means that the fragments having the same mass (for example $M_H = 148$) can be produced in three different valleys and they will have 3 different deformation sets, and, as consequence 3 sets of $\langle TKE\rangle$, as it was clearly demonstrated in the experiments [55] using ^{210}Po and ^{213}At. In fact this is the essence of the multi-modal approach to the fission process. The question is with what statistical weight every specific mode will contribute into the total $(M - TKE)$ distribution? As mentioned above, this contribution will be determined by the ratio of heights and penetrations of the fission barriers in every valley.

We have not yet finished the calculations for the ^{256}No fission valleys, the results will shortly be published elsewhere. However according to the preliminary data, the valley A is the first candidate for the population in the fission process. As one can see in Fig. 23, the bottom of this valley corresponds to the fragments with masses $M \approx 135 - 145$, and a more probable nuclear shape near the scission point is shown in Fig. 24(A). In this case the shape of the heavy fragment is close to the spherical one, and the deformation of the en-tire fissioning nucleus is quite compact. It corresponds to the fission of ^{256}No in a standard asymmetric valley and this is in excellent agreement with the experimental data on the spontaneous fission of ^{256}No (fig. 8(a) from [119]), as well as with our results. Comparing the potential energy in different valleys, valley B is situated quite high (see Fig. 23), and its more probable nuclear shape is presented in Fig. 24(B). It is the Super-Short (SS) valley with very compact shapes of both fragments and mass of heavy fragment $M_H \approx 134$, that also agrees well with our experimental results. However, as the calculations show, such a compact shape is extremely unstable with respect to small changes in the deformation, and the nucleus tends to take shape A, since the light fragment is far from being magic in the neutron number. Therefore, the evolution of the fission process along valley B is unlikely, and the yield of the SS-mode fragments should be small, as we have observed in the experiment.

In valleys C and D (Fig. 23) the fragments are strongly deformed, and the most probable shapes, corresponding to the division into masses 122/134 and 95/161, are shown in Fig. 24(C) and (D). Although valley C has the minimum of the potential energy corresponding to mass $M_H \approx 134$, it is not connected with the spherical shells $Z = 50$ and $N = 82$. The fragment shapes are so strongly deformed, that by their shapes they are close to those obtained in the LDM [125], and all the properties of the valley are mainly due to the liquid-drop component of the potential energy, but "distorted" by the strongly deformed shells, as it was shown for the pre-actinide nucleus in [126]. In Brosa's

terminology, this valley as well as the corresponding mode is called the Super-Long (SL) mode. In spontaneous and low-energy fission this mode practically does not manifest itself. With increasing excitation energy, its properties become similar to those in the LDM, as it happens in our experiment (Figs. 6 and 7)

Valley D is formed by the light fragment cluster, whose properties are close to those of the third standard mode S3 recently found in ref. [80], in which the neutron number in the light fragment $N \approx 52$ [80] or slightly more [127]. This mode is a very asymmetric one and difficult to observe in the experimental mass distributions. In our case it is just the statistical accuracy that is lacking.

Finally, the shapes of the fissioning nucleus for mass $M_H = 148$, produced in three different valleys C, D and A are compared in Fig. 24(E+F) and Fig. 24(F+G). This presents a good example of the fission modality. Thus, our theoretical studies explain clearly the main properties and the regularities of the low-energy fission of ^{256}No investigated experimentally.

VI. CONCLUSIONS

For the reaction ^{48}Ca $+^{208}$Pb$\rightarrow^{256}$No, the capture-fission cross-sections and the mass energy distributions have been measured for the energies of ^{48}Ca-projectiles respectively from 206 up to 242 MeV and from 211 up to 242 MeV with the help of the CORSET double-arm time-of-flight spectrometer. The MED of fragments for heated fission has been shown to consist of two components. One of the components is classical fusion component due to the symmetric fission of the ^{256}No compound nucleus, and the other component, which manifests itself as "quasi-fission shoulders", is associated with a quasi-fission process. The quasi-fission shoulders, which embrace light fragments of a mass of $\sim 60-90$, show increased TKE as compared with that expected for a FF process. The conclusion has been drawn, in agreement with work [54], that in QF, the spherical shells with $Z = 28$ and $N = 50$ play a key role. This conclusion is supported by results from work [83]. The MD of fragments for the ^{40}Ar $+^{208}$Pb$\rightarrow^{248}$Fm reaction obtained in this work has marked quasi-fission shoulders whose characteristics are close to those of the quasi-fission shoulders associated with the reaction ^{48}Ca $+^{208}$Pb $\rightarrow^{256}$No. The properties of MED of fragments have also been demonstrated to formally fit the standard hypothesis about two independent fission modes; in this case, the two modes are only a normal FF process and a QF process, which exhibit their features.

A version of the Dinuclear System model has been developed, which has enabled the experimental energy dependences of the capture-fission cross-sections and the xn-channels of the reaction concerned to be described. This version of the DNS model, which takes account of shell effects, provides qualitatively correct predictions about the mass distribution for QF.

A comparison of the mass distributions for QF measured in experiment and calculated by the dynamical transport model [92] shows that this model also provides qualitatively correct predictions. However both models need improving to a large measure to provide quantitative predictions.

It has been found that at low excitation energies, there exists a high energy Super-Short mode of classical fission in the mass region of heavy fragments $M = 130-135$, the $TKE \approx 233$ MeV, but the yield of this mode is small. Its properties can be accounted for with the help of the classical modal approach, which is based on the fact that the potential energy surface in the deformation space of the fissioning nucleus has valley structure.

Acknowledgments

We are pleased to acknowledge help from Dr. V. S. Salamatin in data processing and advices from Prof. V. V. Volkov in conducting theoretical investigations. One of us, (C. E. A), thanks Prof. V. I. Zagrebaev for his program for calculating driving potential and numerous helpful and fruitful discussions. P. E. V. thanks Prof. F. Hanappe for helpful discussions. This work was supported by the Russian Foundation for Basic Research under Grant No. 03-02-16779, and by INTAS grants YS 2002-261 and partly No. 00-655.

[1] Yu. A. Lazarev, Yu. V. Lobanov, Yu. Ts. Oganessian, V. K. Utyonkov, F. Sh. Abdulin, A. N. Polyakov, J. Rigol, I. V. Shirokovsky, Yu. S. Tsyganov, S. Iliev, V. G. Subbotin, A. M. Sukhov, G. V. Buklanov, B. N. Gikal, V. N. Kutner, A. N. Mezentsev, K. Subotic, J. F. Wild, R. W. Lougheed, and K. J. Moody, Phys. Rev. C **54**, 620 (1996); S. Hofmann, Rep. Prog. Phys. **61**, 639 (1998). S. Hofmann and G. Münzenberg, Rev. Mod. Phys. **72**, 733 (2000). P. Armbruster, Annu. Rev. Nucl. Part. Sci. **50**, 411 (2000).

[2] Yu. Ts. Oganessian, A. V. Yeremin, G. G. Gulbekian, S. L. Bogomolov, V. I. Chepigin, B. N. Gikal, V. A. Gorshkov, M. G. Itkis, A. P. Kabachenko, V. B. Kutner, A. Yu. Lavrentev, O. N. Malyshev, A. G. Popeko, J. Roháč, R. N. Sagaidak, S. Hofmann, G. Münzenbeg, M. Veselsky, S. Saro, N. Iwasa, and K. Morita, Eur. Phys. J. A **5**, 63 (1999).

[3] Yu. Ts. Oganessian, A. V. Yeremin, A. G. Popeko, S. L. Bogomolov, G. V. Buklanov, M. L. Chelnokov, V. I. Chepigin, B. N. Gikal, V. A. Gorshkov, G. G. Gulbekian, M. G. Itkis, A. P. Kabachenko, A. Yu. Lavrentev, O. N. Malyshev, J. Roháč, R. N. Sagaidak, S. Hofmann, S. Saro, G. Giardina, and K. Morita, Nature, **400**, 242 (1999). Yu. Ts. Oganessian, V. K. Utyonkov, Yu. V. Lobanov, F. Sh. Abdulin, A. N. Polyakov, I. V. Shirokovsky, Yu. S. Tsyganov, G. G. Gulbekian, S. L. Bogomolov, B. N. Gikal, A. N. Mezentsev, S. Iliev, V. G. Subbotin, A. M. Sukhov, G. V. Buklanov, K. Subbotic, M. G. Itkis, K. J. Moody, J. F. Wild, N. J. Stoyer, M. A. Stoyer, and R. W. Lougheed, Phys. Rev. Lett. **83**, 3154 (1999); Phys. Rev. C **62**, (2000) 041604(R); Phys. Rev. C **63**, 011301(R) (2001).

[4] W. D. Myers, and W. J. Swiatecki, Nucl. Phys. **81**, 1 (1966); A. Sobiczewski, F. A. Gareev, and B. N. Kalinkin, Phys. Lett. **22**, 500 (1966); P. Möller and J. R. Nix, J. Phys. G **20**, 1681 (1994); R. Smolanczuk, J. Skalski and A. Sobiczewski, Phys. Rev. C **52**, 1871 (1995); R. Smolanczuk, Phys. Rev. C **56**, 812 (1997); S. Ćwiok, J. Dobaczewski, P.-H. Heenen, P. Magierski, and W. Nazarewicz, Nucl. Phys. **A611**, 211 (1996); T. Bürvenich, K. Rutz, M. Bender, P.-G. Reinhard, J. A. Maruhn, and W. Greiner, Eur. Phys. J. A **3**, 139 (1998); S. Ćwiok, W. Nazarewicz, and P.-H. Heenen, Phys. Rev. Lett. **83**, 1108 (1999); M. Bender, K. Rutz, P.-G. Reinhard, J. A. Maruhn, and W. Greiner, Phys. Rev. C **60**, 034304 (2000); M. Bender, Phys. Rev. C **61**, 031302 (2000); A. T. Kruppa, M. Bender, W. Nazarewicz, P.-G. Reinhard, T. Vertse, and S. Ćwiok, Phys. Rev. C **61**, 034313 (2000).

[5] R. Bock, Y. T. Chu, M. Dakowski, A. Gobbi, E. Grosse, A. Olmi, H. Sann, D. Schwalm, U. Lynen, W. Müller, S. Bjørnholm, H. Esbensen, W. Wölfli, and E. Morenzoni, Nucl. Phys. **A388**, 334 (1982).

[6] G. Guarino, A. Gobbi, K. D. Hildenbrand, W. F. J. Müller, A. Olmi, A. Sann, S. Bjørnholm, and G. Rudolf, Nucl. Phys. **A424**, 157 (1984).

[7] J. Töke, R. Bock, G. X. Dai, S. Gralla, A. Gobbi, K. D. Hildenbrand, J. Kuzminski, W. F. J. Müller, A. Olmi, H. Stelzer, B. B. Back, and S. Bjørnholm, Nucl. Phys. **A440**, 327 (1985).

[8] W. Q. Shen, J. Albinski, A. Gobbi, S. Gralla, K. D. Hildenbrand, N. Herrmann, J. Kuzminski, W. F. J. Müller, A. Olmi, H. Stelzer, J. Töke, B. B. Back, S. Bjørnholm, and S. P. Sørensen, Phys. Rev. C **36**, 115 (1987).

[9] R. Kalpakchieva, Yu. Ts. Oganessian, Yu. E. Penionshkevitch, V. N. Polyansky, H. Bruchertseifer, K. A. Gavrilov, and Choi Val Sek, Yad. Fiz. **26**, 253 (1977).

[10] A. J. Pacheco, J. O. Fernandez Niello, D. E. DiGrigorio, M. di Tada, J. E. Testoni, Y. Chan, E. Chavez, S. Gazes, E. Plagnol, and R. G. Stokstad, Phys. Rev. C **45**, 2861 (1992).

[11] R. Kalpakchieva, Yu. Ts. Oganessian, Yu. E. Penionzhkevich, H. Sodan, and B. A. Gvozdev, Phys. Lett. B **69**, 287 (1977).

[12] Yu. Ts. Oganessian, A. G. Demin, A. S. Iljinov, S. P. Tretyakova, A. A. Pleve, Yu. E. Penionzhkevich, M. P. Ivanov, and Yu. P. Tretyakov, Nucl. Phys. **A239** 157, (1975). G. N. Flerov, Yu. Ts. Oganessian, A. A. Pleve, N. V. Pronin, and Yu. P. Tretyakov, Nucl. Phys. **A267**, 359 (1976).

[13] V. B. Kutner, S. L. Bogomolov, A. A. Efremov, A. N. Lebedev, V. Ya. Lebedev, V. N. Loginov, A. B. Yakushev, and N. Yu. Yazvitsky, Rev. Sci. Instr. **71**, 860; 774 (2000).

[14] E. M. Kozulin, N. A. Kondratjev, and I. V. Pokrovski, *Heavy Ion Physics*, Scientific Report 1995-1996 (JINR, FLNR, Dubna, 1997) p. 215; N. A. Kondratiev, E. M. Kozulin, I. V. Pokrovski, and E. V. Prokhorova, in *Proc.4-th Int. Conf. on Dynamical aspects of nuclear fission (DANF'98)*, Časta-Papiernička, Slovak Republic, October 1998 (World Scientific, Singapore, 2000) p. 431.

[15] I. V. Pokrovsky, L. Calabretta, M. G. Itkis, N. A. Kondratiev, E. M. Kozulin, C. Maiolino, E. V. Prokhorova, A. Ya. Rusanov, and S. P. Tretyakova, Phys. Rev. C **60**, 041304 (1999).

[16] M. G. Itkis, Yu. Ts. Oganessian, E. M. Kozulin, N. A. Kondratiev, L. Krupa, I. V. Pokrovski, A. N. Polyakov, V. A. Ponomarenko, E. V. Prokhorova, B. I. Pustylnik, A. Ya. Rusanov, and V. I. Vakatov, Nuovo Cim. A **111**, 783 (1998) .

[17] M. G. Itkis, Yu. Ts. Oganessian, E. M. Kozulin, N. A. Kondratiev, L. Krupa, I. V. Pokrosky, A. N. Polyakov, V. A. Ponomarenko, E. V. Prokhorova, and A. Ya. Rusanov in *Proceedings of 7-th International Conference on Clustering aspects of nuclear structure and dynamics (Claster'99)* Rab Island, Croatia, June 1999 (World Scientific, Singapore 2000) p.386.

[18] G. G. Chubaryan, M. G. Itkis, S. M. Lukyanov, V. N. Okolovich, Yu. E. Penionzhkevich, V. S. Salamatin, A. Ya. Rusanov, and G. N. Smirenkin, Phys. At. Nucl. **56**, 286 (1993).

[19] M. G. Itkis, N. A. Kondratiev, E. M. Kozulin, Yu. Ts. Oganessian, I. V. Pokrovsky, E. V. Prokhorova, and A. Ya. Rusanov, Phys. Rev. C **59**, 3172 (1999).

[20] A. V. Yeremin, V. I. Chepigin, M. G. Itkis, A. P. Kabachenko, S. P. Korotkov, O. N. Malyshev, Yu. Ts. Oganessian, A. G. Popeko, J. Roháč, R. N. Sagaidak, M. I. Chelnokov, V. A. Gorshkov, A. Yu. Lavrentev, S. Hofmann, G. Münzenbeg, M. Veselsky, S. Saro, K. Morita, N. Iwasa, S. I. Mulgin and S. V. Zhdanov, JINR Rapid Communications No.6 [92]-98 (JINR, Dubna 1998) p. 21; A. V. Belozerov, M. L. Chelnokov, V. I. Chepigin, T. P. Drobina, V. A. Gorshov, A. P. Kabachenko, O. N. Malyshev, I. M. Merkin, Yu. Ts. Oganessian, A. G. Popeko, R. N. Sagaidak, A. I. Svirikhin, A. V. Yeremin, G. Berek, I. Brida, and S. Saro, Eur. Phys. J. A **16**, 447 (2003).

[21] J. R. Nix and W. J. Swiatecki, Nucl. Phys. **71**, 1 (1965); J. R. Nix, Nucl. Phys. **A130**, 241 (1969).

[22] G. D. Adeev, I. I. Gonchar, V. V. Pashkevich, N. I. Pischasov, and O. I. Serdyuk, Sov. J. Part. Nucl. **19**, 529 (1988); G. D. Adeev, and V. V. Pashkevich, Nucl. Phys. **A502**, 405c (1989).

[23] M. G. Itkis, S. M. Lukyanov, V. N. Okolovich, Yu. E. Penionzhkevich, A. Ya. Rusanov, V. S. Salamatin, G. N. Smirenkin, and G. G. Chubaryan, Sov. J. Nucl. Phys. **52**, 15 (1990).

[24] M. G. Itkis, and A. Ya. Rusanov, Phys. Part. Nucl. **29**, 160 (1998).

[25] A. V. Antonenko, E. A. Cherepanov, A. K. Nasirov, V. P. Permjakov, and V. V. Volkov, Phys. Lett. B **319**, 425 (1993); Phys. Rev. C **51**, 2635 (1995).
[26] G. G. Adamian, N. V. Antonenko, W. Scheid, and V. V. Volkov, Nucl. Phys. **A618**, 176 (1997); Nucl. Phys. **A633**, 409 (1998);
[27] G. G. Adamian, N. V. Antonenko, and W. Scheid, Nucl. Phys. **A627**, 361 (1997).
[28] E. A. Cherepanov, Pramana - J. Phys. **53**, 619 (1999).
[29] A. S. Iljinov, and E. A. Cherepanov, JINR Communication, P7-84-68, (JINR, Dubna 1984) (in Russian).
[30] W. J. Swiatecki, Phys. Scripta **24**, 113 (1981); S. Bjørnholm, and W. J. Swiatecki, Nucl. Phys. **A319**, 471 (1982); J. P. Blocki, H. Feldmeier, and W. J. Swiatecki, Nucl. Phys. **A459**, 145 (1986).
[31] J. P. Blocki, J. Randrup, W. J. Swiatecki, and C. F. Tsang, Ann. Phys. (N.Y.) **105**, 427 (1977).
[32] L. G. Moretto, and J. S. Sventek, Phys. Lett. B **58**, 26 (1975).
[33] E. A. Cherepanov, A. S. Iljinov, and M. V. Mebel, J. Phys. G **9**, 931 (1983).
[34] T. Sikkeland, Ark. Fys. **36**, 539 (1967).
[35] V. I. Zagrebaev, in *Proc. Int. Workshop on Fusion Dynamics at the Extremes*, Dubna, Russia, May 2000 (World Scientific, Singapore 2001) p. 215.
[36] M. Ohta, ibid., p.110.
[37] T. Ericson, and V. M. Strutinski, Nucl. Phys. **8**, 284 (1958).
[38] V. S. Barashenkov and V. D. Toneev, *Interaction of High Energy Particle with Atomic Nuclei* (Atomizdat, Moscow, 1972) (in Russian).
[39] I. Dostroovsky, Z. Fraenkel, and G. Friendlander, Phys. Rev. **116**, 683 (1959).
[40] A. S. Iljinov, Yu. Ts. Oganessian, and E. A. Cherepanov, Sov. J. Nucl. Phys. **33**, 520 (1981).
[41] A. V. Ignatyuk, *Statistical Properties of Excited Atomic Nuclei.* (Energoatomizdat, Moscow, 1983) (in Russian). [translated as IAEA report INDC(CCP)-233/L, Vienna, 1985].
[42] E. A. Cherepanov, and A. S. Iljinov, Nukleonika, **25**, 611 (1980).
[43] W. D. Myers and W. J. Swiatecki, Ark. Fys. **36**, 343 (1967).
[44] E. A. Cherepanov, in *Proceedings of the International Conference on Beam Nuclear Spectorscopy*, Debrecen, Hungary, May 1984 (House of the Hungarian Academy of Sciences, 1984) p. 499.
[45] V. S. Barashenkov, F. G. Zheregy, A. S. Iljinov, and V. D. Toneev, Sov. J. Part. Nucl. **5**, 469 (1974).
[46] E. A. Cherepanov, A. S. Iljinov, and M. V. Mebel, J. Phys. G **9**, 1397 (1983).
[47] Y. Aritomo, T. Wada, and M. Ohta, See Ref. [35], p. 123.
[48] H. Keller, K. Lützenkirchen, J. V. Kratz, G. Wirth, W. Brüchle, and K. Sümmerer, Z. Phys. A **326**, 313 (1987).
[49] K. Lützenkirchen, J. V. Kratz, G. Wirth, W. Brüchle, L. Dörr, K. Sümmerer, R. Lucas, J. Poitou, C. Gregoire, and S. Bjørnholm, Z. Phys. A **320**, 529 (1985) .
[50] G. Wirth, W. Brüchle, K. Sümmerer, R. Lucas, J. Poitou, and C. Gregoire, Nucl. Phys. **A452**, 351 (1986).
[51] H. Schulte, B. Jäckel, R. A. Esterlund, M. Knaack, W. Westmeier, A. Rox, and P. Patzelt, Phys. Lett. B **232**, 37 (1989).
[52] P. Klein, J. V. Kratz, M. K. Gober, H. P. Zimmermann, W. Brüchle, W. Reisdorf, and M. Schädel, Z. Phys. A **357**, 193 (1997).
[53] B. Jäckel, A. Rox, R. A. Esterlund, W. Westmeier, M. Knaack, and P. Patzelt, Z. Phys. A **339**, 475 (1991) .
[54] A. Yu. Chizhov, M. G. Itkis, I. M. Itkis, G. N. Kniajeva, E. M. Kozulin, N. A. Kondratiev, I. V. Pokrovsky, R. N. Sagaidak, V. M. Voskressensky, A. V. Yeremin, L. Corradi, A. Gadea, A. Latina, A. M. Stefanini, S. Szilner, M. Trotta, A. M. Vinodkumar, S. Beghini, G. Montagnoli, F. Scarlassara, A. Ya. Rusanov, F. Hanappe, O. Dorvaux, N. Rowley, and L. Stuttge, Phys. Rev. C **67**, 011603(R) (2003).
[55] M. G. Itkis, V. N. Okolovich, A. Ya. Rusanov, and G. N. Smirenkin, Sov. J. Part. Nucl. **19**, 301 (1988).
[56] F. Plasil, D. S. Burnet, H. C. Britt, and S. G. Thompson, Phys. Rev. **142**, 696 (1966).
[57] R. L. Ferguson, F. Plasil, H. Freisleben, C. E. Bemis, and H. W. Schmitt, Phys. Rev. C **8**, 1104 (1973).
[58] B. G. Glagola, B. B. Back, and R. Betts, Phys. Rev. C **29**, 486 (1984).
[59] L. G. Sobotka, D. G. Sarantites, Ze Li, E. N. Dines, M. L. Halbert, D. C. Hensley, R. P. Schmitt, Z. Majka, G. Nebbia, H. C. Griffin, and A. J. Sierk, Nucl. Phys. **A471**, 131c (1987); Phys. Rev. C **36**, 2713 (1987).
[60] W. U. Schröder, and J. R. Huizenga, Nucl. Phys. **A502**, 473c (1989).
[61] M. G. Itkis, Yu. A. Muzychka, Yu. Ts. Oganessian, V. N. Okolovich, V. V. Pashkevich, A. Ya. Rusanov, V. S. Salamatin, G. N. Smirenkin, and G. G. Chubarian, Phys. At. Nucl. **58**, 2026 (1995).
[62] B. B. Back, P. B. Fernandez, B. G. Glagola, D. Henderson, S. Kaufman, J. G. Keller, S. J. Sanders, F. Videbaek, T. F. Wang, and B. D. Wilkins, Phys. Rev. C **53**, 1734 (1996).
[63] A. Ya. Rusanov, M. G. Itkis, and V. N. Okolovich, Phys. At. Nucl. **60**, 683 (1997).
[64] A. I. Startsev, in *Proceedings of the XIII Meeting on Physics of Nuclear Fission in Memory of Prof. G. N. Smirenkin*, Obninsk, Kaluga Region, Russia, October 1995. Edited by B. D. Kuzminov (IPPE, Obninsk, 1995) p. 94 (in Russian); A. I. Startsev, Proc. VI International School-Seminar on Heavy Ion Physics, Dubna, Russia, September 1997. Editors Yu. Ts. Oganessian and R. Kalpakchieva (World Scientific, Singapore, 1998) p. 637.
[65] D. V. Vanin, G. I. Kosenko, and G. D. Adeev, Phys. Rev. C **59**, 2114 (1999).
[66] A. V. Karpov, P. N. Nadtochy, D. V. Vanin, and G. D. Adeev, Phys. Rev. C **63**, 054610 (2001).
[67] P. N. Nadtochy, G. D. Adeev, and A. V. Karpov, Phys. Rev. C **65**, 064615 (2002).
[68] A. Ya. Rusanov, V. V. Pashkevich, and M. G. Itkis, Phys. At. Nucl. **62**, 547 (1999).
[69] J. G. Keller, B. B. Back, B. G. Glagola, D. Henderson, S. B. Kaufman, S. J. Sanders, R. H. Siemssen, F. Videbaek, B. D. Wilkins, and A. Worsham, Phys. Rev. C **36**, 1364 (1987).

[70] P. Möller, J. R. Nix, W. D. Myers, and W. J. Swiatecki, At. Data Nucl. Data Tabl. **59**, 185 (1995).
[71] A. V. Ignatyuk, G. N. Smirenkin, M. G. Itkis, S. I. Mulgin, and V. N. Okolovich, Sov. J. Part. Nucl. **16**, 307 (1985).
[72] V. M. Strutinsky, Sov. J. Nucl. Phys. **1**, 588 (1965).
[73] S. Cohen, F. Plasil, and W. J. Swiatecki, Ann. Phys. (N.Y.) **82**, 557 (1964).
[74] A. J. Sierk, and J. R. Nix, Phys. Rev. C **21**, 982 (1980).
[75] S. V. Zhdanov, M. G. Itkis, S. I. Mulgin, V. N. Okolovich, A. Ya. Rusanov, G. N. Smirenkin, and M. I. Subbotin, Sov. J. Nucl. Phys. **55**, 1766 (1992); Phys. At. Nucl. **56**, 175 (1993).
[76] G. I. Kosenko, I. I. Gonchar, O. I. Serdyuk, and N. I. Pischasov, Sov. J. Nucl. Phys. **55**, 514 (1992).
[77] D. Hilscher and H. Rossner, Ann. Phys. (Fr.) **17**, 471 (1992).
[78] H. C. Britt, H. E. Wegner, and J. C. Gursky, Phys. Rev. **129**, 2239 (1963).
[79] M. G. Itkis, V. N. Okolovich, A. Ya. Rusanov, and G. N. Smirenkin, Z. Phys. A **320**, 433 (1985).
[80] S. I. Mulgin, V. N. Okolovich, and S. V. Zhdanov, Phys. Lett. B **462**, 29 (1999).
[81] F. L. H. Wolfs, Phys. Rev. C **36**, 1379 (1987).
[82] J. Gehring, B. B. Back, K. C. Chan, M. Freer, D. Henderson, C. L. Jiang, K. E. Rehm, J. P. Schiffer, M. Wolanski, and A. H. Wuosmaa, Phys. Rev. C **55**, 2959 (1997).
[83] D. J. Hinde, D. Hilscher, H. Rossner, B. Gebauer, M. Lehmann, and M. Wilpert, Phys. Rev. C **45**, 1229 (1992).
[84] J. Welkovska, C. R. Morton, R. L. McGrath, P. Chung, and I. Dioszegi, Phys. Rev. C **59**, 1506 (1999).
[85] M. A. Butler, S. S. Datta, R. T. de Souza, J. R. Huizenga, W. U. Schröder, J. Töke, and J. L. Wile, Phys. Rev. C **34**, 2016 (1986).
[86] R. Kalpakchieva, Yu. Ts. Oganessian, Yu. E. Penionzhkevich, and H. Sodan, Z. Phys. A **283**, 253 (1977).
[87] G. J. Mathews, L. G. Sobotka, G. J. Wozniak, R. Regimbart, R. P. Schmitt, G. U. Rattazzi, and L. G. Moretto, Z. Phys. A **290**, 407 (1979).
[88] P. Gippner, K. D. Schilling, W. Seidel, F. Stary, E. Will, H. Sodan, S. M. Lukyanov, V. S. Salamatin, Yu. E. Penionzhkevich, G. G. Chubarian, and R. Schmidt, Z. Phys. A **325**, 335 (1986).
[89] M. G. Itkis, Yu. Ts. Oganessian, A. A. Bogachev, I. M. Itkis, M. Jandel, J. Kliman, G. N. Kniajeva, N. A. Kondratiev, I. V. Korzyukov, E. M. Kozulin, L. Krupa, I. V. Pokrovski, E. V. Prokhorova, A. Ya. Rusanov, V. M. Voskresenski, F. Hanappe, B. Benoit, T. Materna, N. Rowley, L. Stuttge, G. Giardina, and K. J. Moody, in *Proceedings of the International Workshop on Fusion Dynamics at the Extremes*, Dubna, Russia, May 2000, edited by Yu. Ts. Oganessian and V. I. Zagrebaev (World Scientific, Singapore, 2001) p. 93-109.
[90] M. G. Itkis, A. A. Bogachev, I. M. Itkis, M. Jandel, J. Kliman, G. N. Kniajeva, N. A. Kondratiev, I. V. Korzyukov, E. M. Kozulin, L. Krupa, Yu. Ts. Oganessian, I. V. Pokrovski, E. V. Prokhorova, A. Ya. Rusanov, V. M. Voskresenski, A. A. Goverdovski, F. Hanappe, T. Materna, N. Rowley, L. Stuttge, G. Giardina, and K. J. Moody, J. Nucl. Radiochem. Sci. **3**, 57 (2002).
[91] A. Diaz-Torres, G. G. Adamian, N. V. Antonenko, and W. Scheid, Nucl. Phys. **A679**, 410 (2001).
[92] A. Diaz-Torres, G. G. Adamian, N. V. Antonenko, and W. Scheid, Phys. Rev. C **64**, 024604 (2001).
[93] V. I. Zagrebaev, Phys Rev. C **64**, 034606 (2001).
[94] E. K. Hulet, J. F. Wild, R. J. Dougan, R. W. Lougheed, J. H. Landrum, A. D. Dougan, M. Schadel, R. V. Hahn, P. A. Baisden, C. M. Henderson, R. J. Dupzyk, K. S E. K. Hulet, J. F. Wild, R. J. Dougan, R. W. Lougheed, J. H. Landrum, A. D. Dougan, M. Schadel, R. V. Hahn, P. A. Baisden, C. M. Henderson, R. J. Dupzyk, K. Sümmerer, and G. R. Bethune, Phys. Rev. Lett, **56**, 313 (1986); Phys. Rev. C **40**, 770 (1989).
[95] E. K. Hulet, Phys. At. Nucl. **57**, 1099 (1994).
[96] M. R. Lane, K. E. Gregorich, D. M. Lee, M. F. Mohar, M. Hsu, C. D. Kacher, B. Kadkhodayan, M. P. Neu, N. J. Stoeyr, E. R. Sylwester, J. N. Yang, and D. C. Hoffman, Phys. Rev. C **53**, 2893 (1996).
[97] D. C. Hoffman, and M. R. Lane, Radiochim. Acta **70/71**, 135 (1995); D. C. Hoffman, T. M. Hamilton, and M. R. Lane, *Nuclear Decay Modes*, edited by D. N. Poenaru (Institute of Physics Publishing, Bristol, 1996) p. 393.
[98] H. C. Britt, D. C. Hoffman, J. van der Plicht, J. B. Wilhelmy, E. Cheifetz, R. J. Dupzyk, and R. W. Lougheet, Phys. Rev. C **30**, 559 (1984).
[99] J. P. Unik, J. E. Gindler, L. E. Glendenin, K. F. Flynn, A. Gorski, and R. K. Sjoblom, *Proc. 3rd Symp. on physics and chemistry of fission*, Rochester, August 1973, vol.2 (IAEA, Vienna, 1974) p. 19.
[100] R. C. Ragaini, E. K. Hulet, R. W. Lougheed, and J. Wild, Phys. Rev. C **9**, 399 (1974).
[101] W. John, E. K. Hulet, R. W. Lougheed, and J. J. Wesolowski, Phys. Rev. Lett. **27**, 45 (1971).
[102] K. F. Flynn, J. E. Gindler, and L. E. Glendenin, Phys. Rev. C **12**, 1478 (1975).
[103] U. Brosa, S. Grossmann, and A. Müller, Z. Phys. A **325**, 241 (1986).
[104] U. Brosa, S. Grossmann, and A. Müller, Phys. Reports **197**, 167 (1990).
[105] P. Möller, J. R. Nix, and W. J. Swiatecki, Nucl. Phys. **A469**, 1 (1987).
[106] P. Möller, J. R. Nix, and W. J. Swiatecki, Nucl. Phys. **A492**, 349 (1989).
[107] V. V. Pashkevich, Nucl. Phys. **A477**, 1 (1988).
[108] S. Ćwiok, P. Rozmej, A. Sobiczewski, and Z. Patyk, Nucl. Phys. **A491**, 281 (1989); A. Sobiczewski, Phys. Part. Nucl. **25**, 119 (1994).
[109] M. Bender, K. Rutz, P.-G. Reinhard, J. A. Maruhn, and W. Greiner, Phys. Rev. C **58**, 2126 (1998).
[110] P. Möller, D. G. Madland, A. J. Sierk, and A. Iwamoto, Nature **409**, 785 (2001).
[111] M. Warda, J. L. Egido, L. M. Robledo, and K. Pomorski, Phys. Rev. C **66**, 014310 (2002).
[112] T. M. Hamilton, K. E. Gregorich, D. M. Lee, K. R. Czerwinski, N. J. Hannink, C. D. Kacher, B. Kadkhodayan, S. A. Kreek, M. J. Nurmia, M. R. Lane, M. P. Neu, A. Türler, and D. C. Hoffman, Phys. Rev. C **46**, 1873 (1992).

[113] J. F. Wild, J. van Aarle, W. Westmeier, R. W. Lougheed, E. K. Hulet, K. J. Moody, R. J. Dougan, E.-A. Koop, R. E. Glaser, R. Brandt, and P. Patzelt, Phys. Rev. C **41**, 640 (1990).
[114] M. Bolsterli, E. O. Fiset, J. R. Nix, and J. L. Norton, Phys. Rev. C **5**, 1050 (1972);
[115] K. Junker, and J. Hadermann, Z. Phys. A **282**, 391 (1977).
[116] S. Čwiok, V. V. Pashkevich, J. Dudek, and W. Nazarewicz, Nucl. Phys. **A410**, 254 (1983); S. Čwiok, Z. Lojewski and V. V. Pashkevich, Nucl. Phys. **A444**, 1 (1985).
[117] P. Reiter, T. L. Khoo, T. Lauritsen, C. J. Lister, D. Seweryniak, A. A. Sonzogni, I. Ahmad, N. Amzal, P. Bhattacharyya, P. A. Butler, M. P. Carpenter, A. J. Chewter, J. A. Cizewski, C. N. Davids, K. Y. Ding, N. Fotiades, J. P. Greene, P. T. Greenlees, A. Heinz, W. F. Henning, R.-D. Herzberg, R. V. F. Janssens, G. D. Jones, H. Kankaanpää, F. G. Kondev, W. Korten, M. Leino, S. Siem, J. Uusitalo, K. Vetter, and I. Wiedenhöver, Phys. Rev. Lett. **84**, 3542 (2000).
[118] J. L. Egido, and L. M. Robledo, Phys. Rev. Lett. **85**, 1198 (2000).
[119] D. C. Hoffman, D. M. Lee, K. E. Gregorich, M. J. Nurmia, R. B. Chadwick, K. B. Chen, K. R. Czerwinski, C. M. Gannett, H. L. Hall, R. A. Henderson, B. Kadkhodayn, S. A. Kreek, and J. D. Leyba, Phys. Rev. C **41**, 631 (1990).
[120] Z. Lojewski, V. V. Pashkevich, and S. Čwiok, Nucl. Phys. **A436**, 499 (1985).
[121] M. G. Itkis, J. V. Kotlov, S. I. Mulgin, V. N. Okolovich, A. Ya. Rusanov, G. N. Smirenkin, and V. N. Tolstikov, Europhys. Lett. **4**, 275 (1987); Sov. J. Nucl. Phys. **46**, 814 (1987).
[122] H. J. Specht, Rev. Mod. Phys. **46**, 733 (1974); Nukleonika, **20**, 717 (1975).
[123] J. Weber, H. C. Britt, A. Gavron, E. Konecny, and J. B. Wilhelmy, Phys. Rev. C **13**, 2413 (1976).
[124] M. Brack, J. Damgaard, A. S. Jensen, H. C. Pauli, V. M. Strutinsky, and C. Y. Wong, Rev. Mod. Phys. **44**, 320 (1972).
[125] G. G. Chubarian, M. G. Itkis, N. A. Kondratiev, E. M. Kozulin, V. V. Pashkevich, I. V. Pokrovsky, A. Ya. Rusanov, V. S. Salamatin, and R. P. Schmitt, Phys. Rev. Lett. **87**, 052701 (2001).
[126] S. I. Mulgin, K.-H. Schmidt, A. Grewe, and S. V. Zhdanov, Nucl. Phys. **A640**, 375 (1998).
[127] I. V. Pokrovsky, M. G. Itkis, I. M. Itkis, N. A. Kondratiev, E. M. Kozulin, E. V. Prokhorova, V. S. Salamatin, V. V. Pashkevich, S. I. Mulgin, A. Ya. Rusanov, S. V. Zhdanov, G. G. Chubarian, B. J. Hurst, R. P. Schmitt, A. Agodi, G. Bellia, L. Calabretta, K. Lukashin, C. Maiolino, A. Kelic, G. Rudolf, L. Stutge, and F. Hanappe, Phys. Rev. C **62**, 014615 (2000).

TABLE I: Characteristics of the reactions and some experimental results.

$E_{\rm lab}$ (MeV)	E^* (MeV)	$\sigma_{\rm c}$ (mb)	$\langle TKE\rangle$ (MeV)	σ^2_{TKE} $(MeV)^2$	$(\sigma^2_M)_G$ $(u)^2$	$\langle\nu_{\rm pre}\rangle$	$T_{\rm cs}$ (MeV)
242	42.8	480 ± 35	195 ± 3	364 ± 17	590 ± 21	1.0	1.93
232	34.7	390 ± 30	198 ± 3	352 ± 18	396 ± 18	0.4	1.89
230	33.1		196 ± 2	340 ± 10	426 ± 15	0.3	1.885
225	29.0	240 ± 22	196 ± 3	310 ± 15	365 ± 22	0	1.88
220	25.0	84 ± 8	197 ± 3	290 ± 15	344 ± 20	0	1.83
217	22.5		196 ± 3	291 ± 17		0	1.81
211	17.6	8 ± 2	195 ± 3	304 ± 24		0	1.75
206	13.6	0.045 ± 0.031					

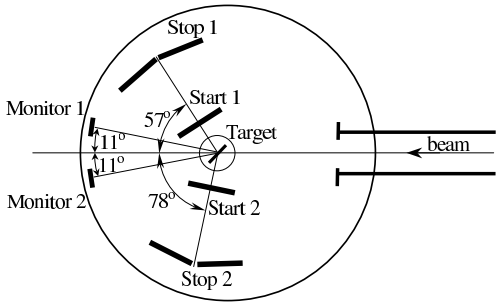

FIG. 1: Schematic diagram of the experimental arrangement

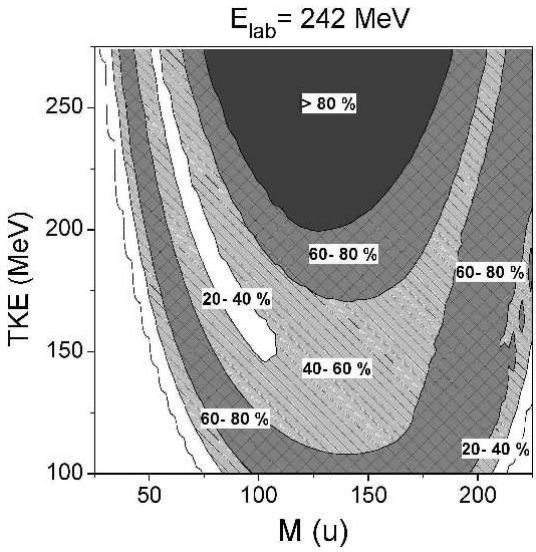

FIG. 2: Geometrical efficiency of the spectrometer (in %) on $(M - TKE)$ coordinates.

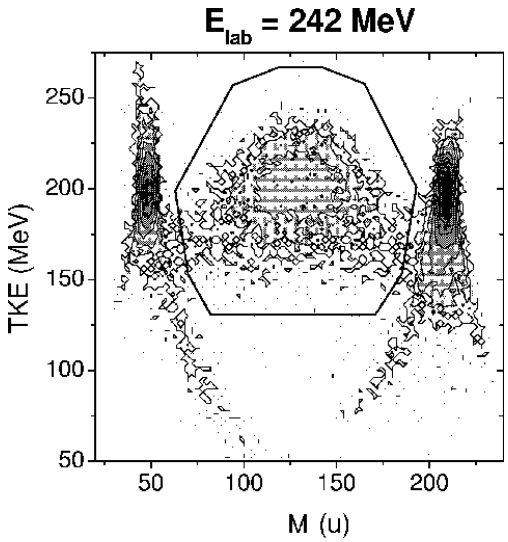

FIG. 3: Two dimensional $(M - TKE)$ matrix for the beam energy $E_{\rm lab} = 242$ MeV without two-body events selection.

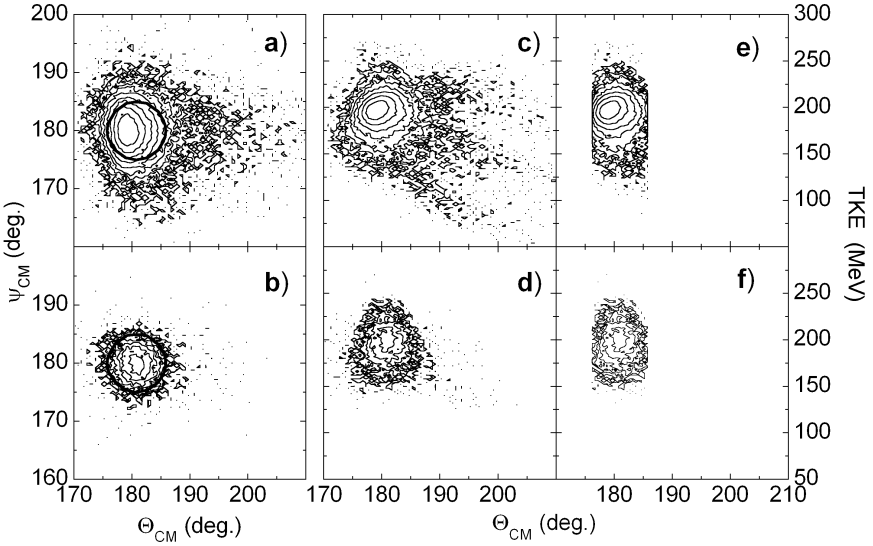

FIG. 4: a) and b) Two-dimensional matrixes for the sum of the center-of-mass angles of divergence of reaction products; $\Theta_{\rm CM}$ – in and $\Psi_{\rm CM}$ – out-of-plane: a) for all the events registered, b) for fission fragments only. Only the events enclosed by curves were analyzed. Figs. c) and d) two-dimensional $\Theta_{\rm CM} - TKE$ matrixes for reaction products; c) for all the events, d) for fragments only. Figs. e) and f) the same as in Figs. c) and d) but only for the events enclosed by curves in Figs. a) and b).

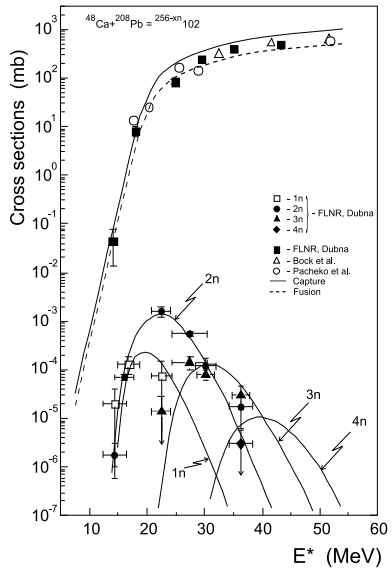

FIG. 5: The dependence of the capture-fission cross-sections σ_c on excitation energy E^*. • - our data, △ – data from ref. [5], ∘ – data from ref.[10]. Shown at the bottom are the data from work [20]on the cross-sections of the xn-channels for the same reaction. The capture-fission cross-sections σ_c and the cross-sections of the xn-channels calculated in the framework of our version of the DNS model are indicated with solid curves. The calculated complete fusion cross-section $\sigma_{\rm CN}$ is indicated with a dashed curve.

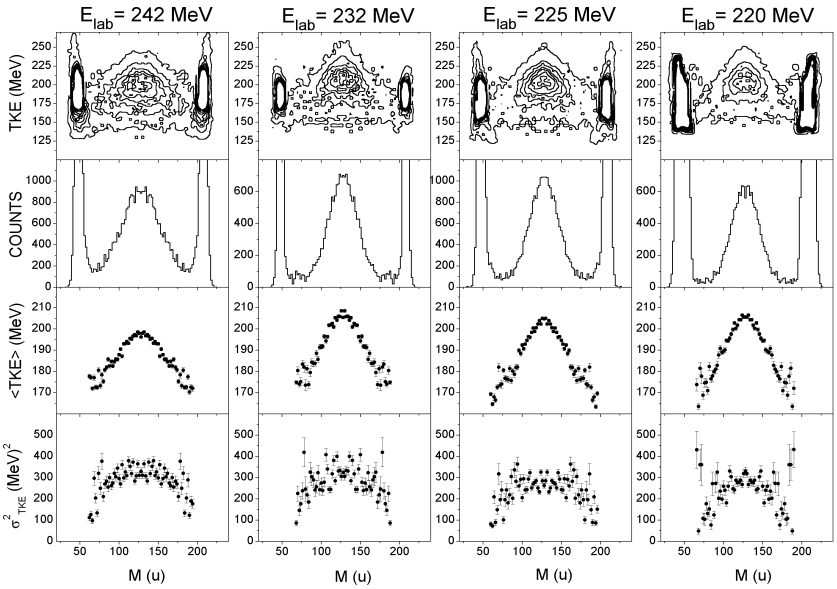

FIG. 6: Shown from top to bottom for the indicated energies of ^{48}Ca-projectiles are: the two-dimensional $(M-TKE)$ reaction product matrixes, the mass distributions and, for fission fragments only, the dependences of $\langle TKE\rangle$ and its variance $\sigma^2_{\rm TKE}$ on fragment mass M.

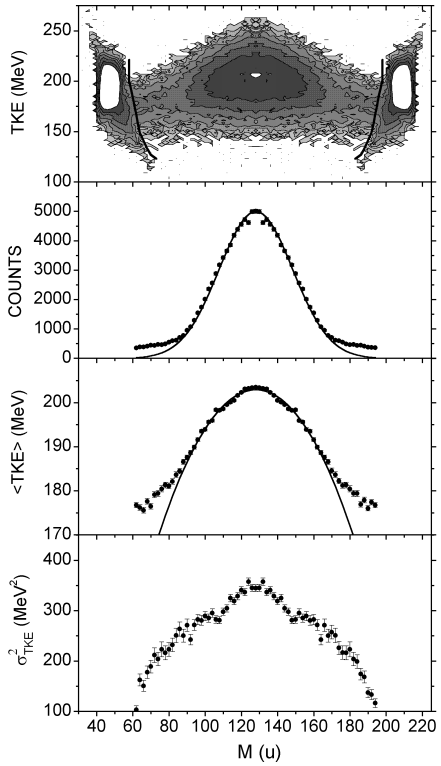

FIG. 7: The same as in Fig.6, but for the energy of ^{48}Ca-ions $E_{\rm lab}$ = 230 MeV. The fragment-like events in the $M-TKE$ matrix are enclosed by solid curves. The characteristics of those fragments are given below.

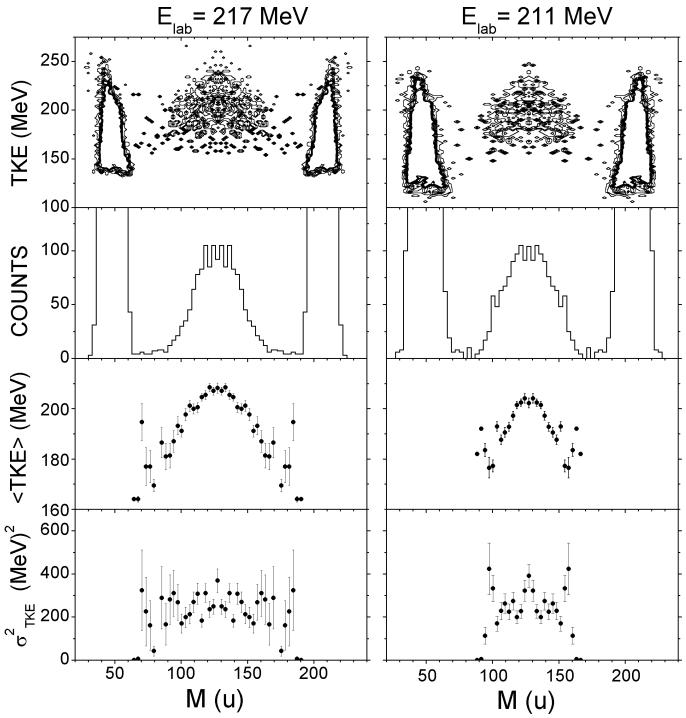

FIG. 8: The same as in Fig. 6, but for the two lowest energies of ^{48}Ca-ions.

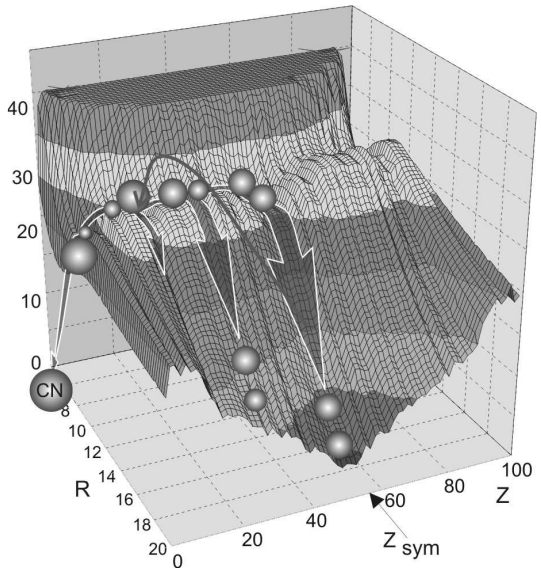

FIG. 9: PROXIMITY potential as a function of the charge number Z and the centre-to-centre distance of fragments. The input channel and the ways for DNS to evolve are indicated with arrows.

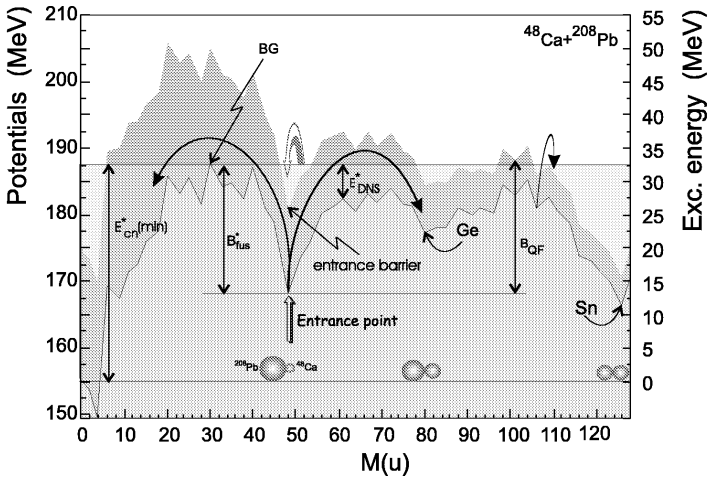

FIG. 10: By way of illustration, the driving potential is shown (lower curve) of the dinuclear system for the reaction ^{48}Ca+^{208}Pb as a function of fragment mass M.

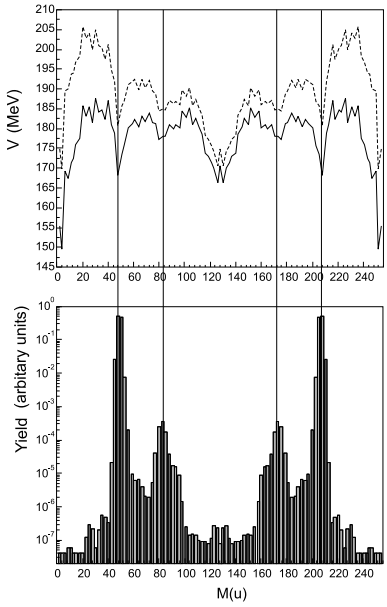

FIG. 11: Driving potential V of the dinuclear system as a function of fragment mass M. Shown below is a calculated mass spectrum for the quasi-fission process occurring in this reaction.

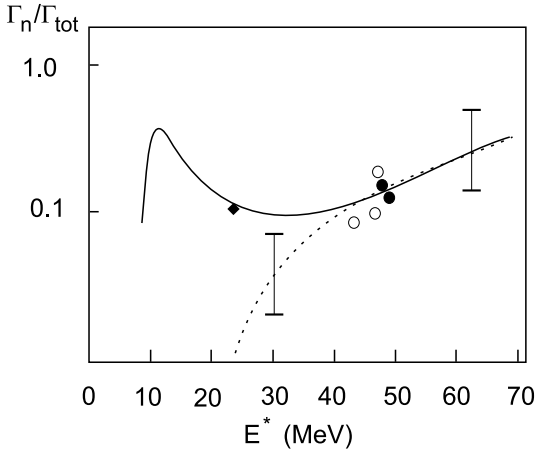

FIG. 12: Probability of neutron emission Γ_n/Γ_{tot} as a function of the E^* of the ^{256}No compound nucleus. The result of calculations taking account of the energy dependence of the shell correction is indicated with a solid curve; the result of calculations on the basis of the liquid-drop fission barrier is indicated with a dotted curve. The figure is taken from ref. [46]; the experimental works from which the experimental data were borrowed are referred to therein.

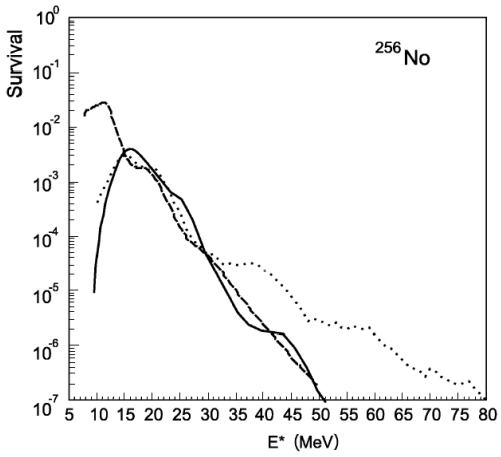

FIG. 13: Survivability of the ^{256}No compound nucleus, calculated by three different approaches, for statistical decay as a function of excitation energy E^*. For details see the text.

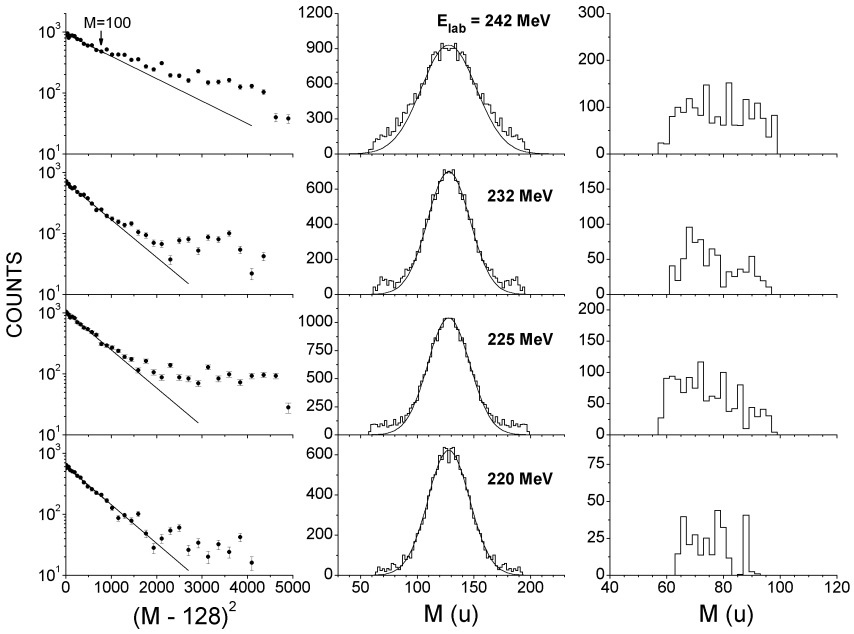

FIG. 14: At the left: Mass yields of fragments as a function of the parameter $(M-128)^2$ (logarithmic scale) for the energies of ^{48}Ca-ions $E_{\rm lab} = 220 - 242$ MeV. On such a scale, a Gaussian is a straight line. At the center: Mass distributions of fragments (linear scale) and fitting Gaussians, as at the left of the figure. At the right: The separated quasi-fission shoulders as a function of the light fragments mass.

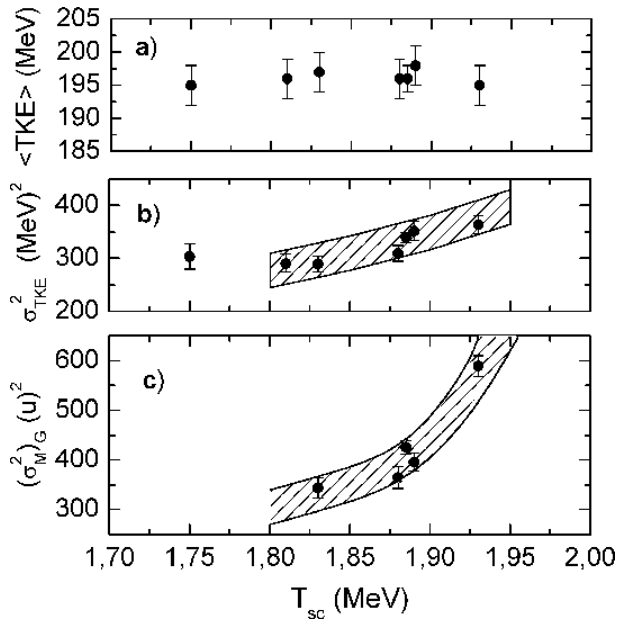

FIG. 15: The dependences of $\langle TKE \rangle$ (a), $\sigma^2_{\rm TKE}$ and $(\sigma^2_M)_G$ on the nucleus temperature at the scission point $T_{\rm sc}$ (21). The regions of $\sigma^2_{\rm TKE}$ and $(\sigma^2_M)_G$ characteristic of classical fission are shown by hatching (see the text).

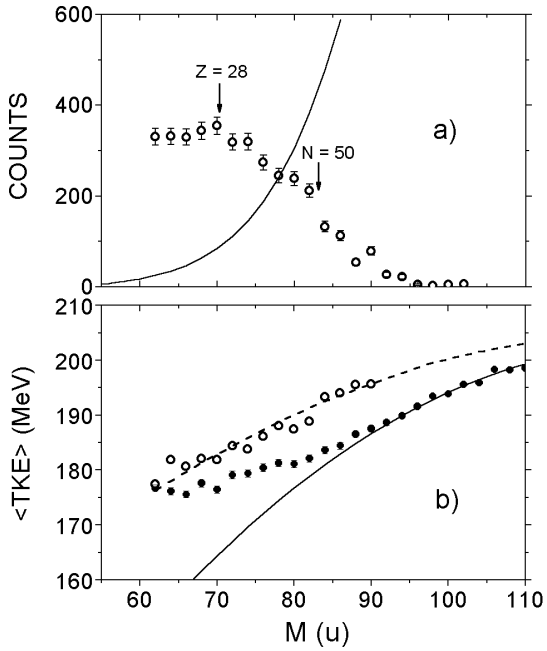

FIG. 16: (a) Yield of the quasi-fission component for the light fragments (open circles). Indicated with a solid curve is a portion of the Gaussian from Fig. 7. The fragment masses with magical Z and N are indicated with arrows; the calculations were done by UCD. (b) M-dependences of the experimental $\langle TKE \rangle$ (black circles) and the TKE of the quasi-fission component (open circles) obtained according to (26). The solid and dotted curves are the fitting parabolic curves for those dependences according to Eq. (27).

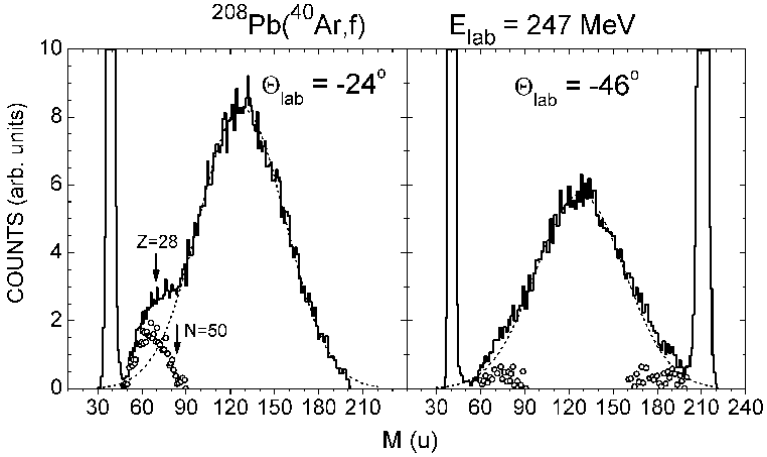

FIG. 17: Mass yields of fragments, presented as a histogram, for the reaction ^{40}Ar+^{208}Pb for two registration angles from work [83]. The fitting Gaussians for FF are indicated with dashed curves. The QF component is indicated with open circles. The fragment masses with magical Z and N, calculated by UCD, are indicated with arrows.

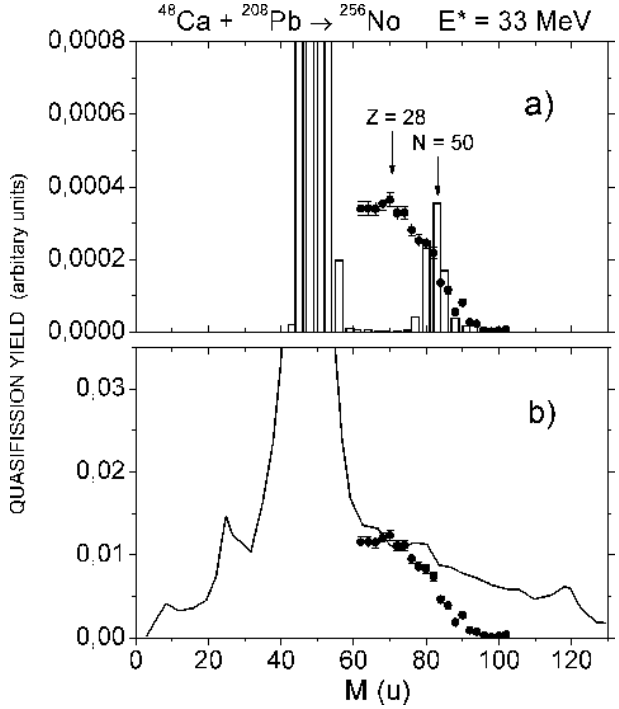

FIG. 18: (a) Comparison of the QF yields obtained in experiment (circles) and calculated by our model (histogram). With arrows, the same is indicated as in Fig 16(a). (b)Comparison of the QF yields obtained in experiment (circles) and calculated in ref. [92] (solid curve).

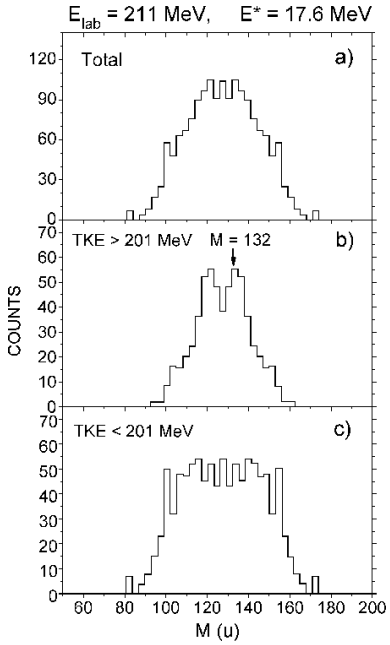

FIG. 19: Fragment mass distributions for $E_{\rm lab} = 211$ MeV ($E^* = 17.6$ MeV): total distribution (a), and differential distributions for $TKE > 201$ MeV(b) and $TKE < 201$ MeV(c).

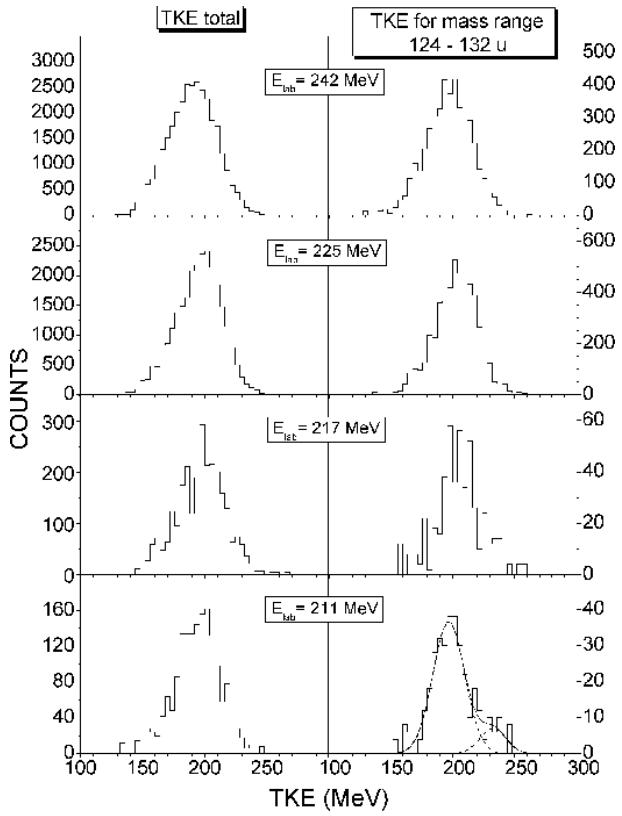

FIG. 20: TKE distributions for four values of the energy of ^{48}Ca-projectiles. At the left: Total distributions; at the right: Differential distributions for the symmetrical mass region $M = 124 - 132$. For the figure on the lower right, fitting Gaussians are shown for two modes.

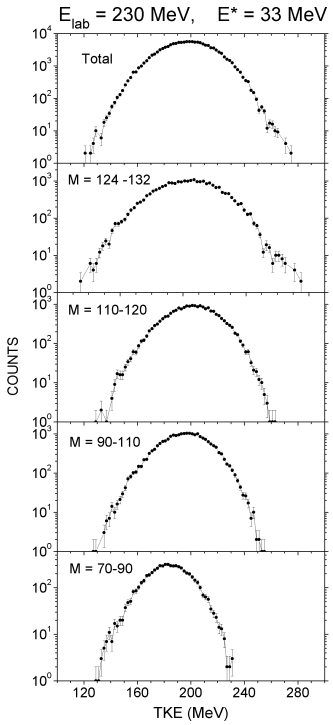

FIG. 21: Total and differential TKE distributions for various mass ranges of fragments at the energy $E_{\rm lab} = 230$ MeV.

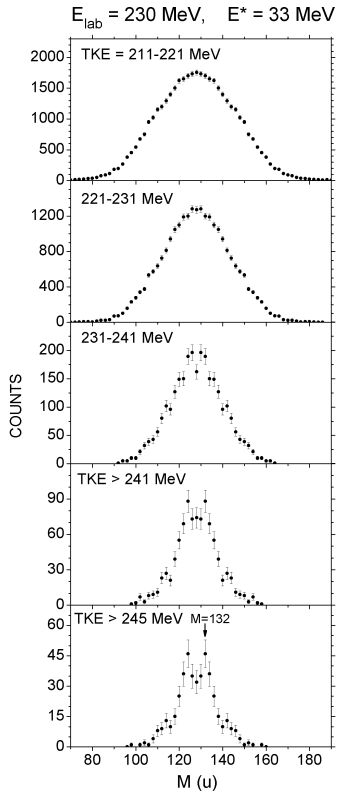

FIG. 22: Fragment mass distribution for different TKE ranges for the beam energy $E_{\rm lab} = 230$ MeV.

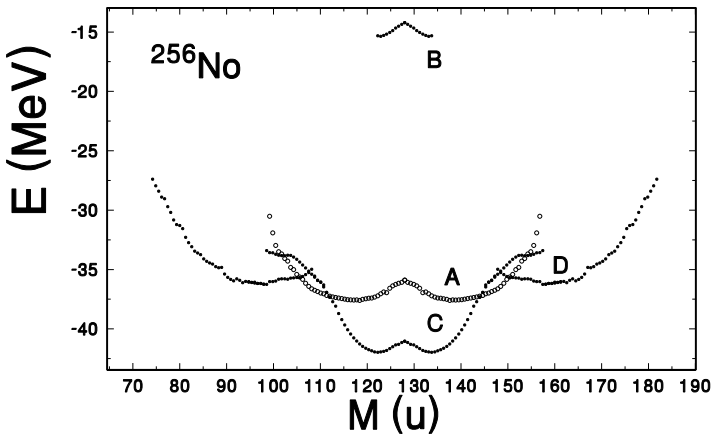

FIG. 23: The ^{256}No fission valleys near the scission point as a function of the fragment mass.

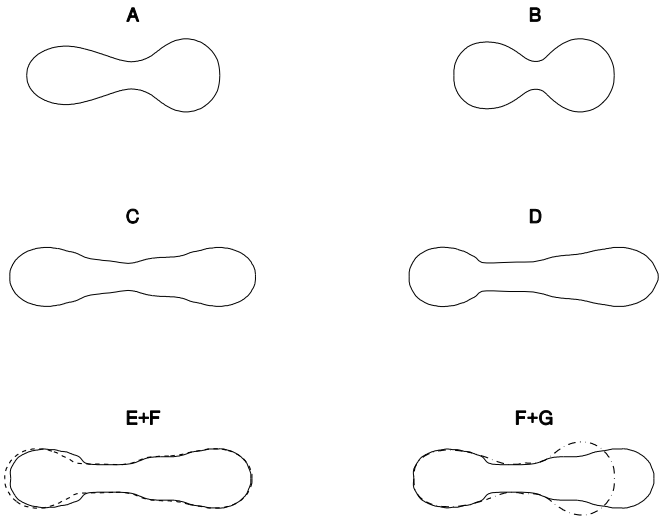

FIG. 24: Shapes of the fragments at the bottom of the valleys shown in Fig. 23, and comparison of the shapes at $M = 148$. Shapes in points E (dashed), F (solid) and G (dash-dotted) stem from the bottoms of the valley C, D and A, respectively, up to the intersection points.